Chinese Journal of Natural Medicines

Zishen Huoxue Decoction alleviates myocardial ischemia–reperfusion injury through dysregulation of endoplasmic reticulum–mitochondria homeostasis mediated by DUSP1–NDUFS4

Xiangyi Pu, Qin Zhang, Zhaoqi Yan, Siyuan Zhou, Qiaomin Wu, Xinai Zhang, Yongyuan Cai, Zhiming Liu, Ruxiu Liu, Xing Chang

Citation: Xiangyi Pu, Qin Zhang, Zhaoqi Yan, Siyuan Zhou, Qiaomin Wu, Xinai Zhang, Yongyuan Cai, Zhiming Liu, Ruxiu Liu, Xing Chang, Zishen Huoxue Decoction alleviates myocardial ischemia–reperfusion injury through dysregulation of endoplasmic reticulum–mitochondria homeostasis mediated by DUSP1–NDUFS4, Chinese Journal of Natural Medicines, 2026, 24(4), 385–401. doi: 10.1016/S1875–5364(26)61171–5.

View online: https://doi.org/10.1016/S1875–5364(26)61171–5

Chinese Journal of Natural Medicines 24 (2026) 385-401

Contents lists available at ScienceDirect

Chinese Journal of Natural Medicines

journal homepage: www.cjnmcpu.com/

Original article

Zishen Huoxue Decoction alleviates myocardial ischemia-reperfusion injury through dysregulation of endoplasmic reticulum-mitochondria homeostasis mediated by DUSP1-NDUFS4

Xiangyi Pu[Δ], Qin Zhang[Δ], Zhaoqi Yan[Δ], Siyuan Zhou, Qiaomin Wu, Xinai Zhang, Yongyuan Cai, Zhiming Liu, Ruxiu Liu[*], Xing Chang[*]

Guang'anmen Hospital, China Academy of Chinese Medical Sciences, Beijing 100053, China

ARTICLE INFO

Article history:
Received 12 February 2025
Revised 8 May 2025
Accepted 14 May 2025
Available online 20 April 2026

Keywords:
Zishen Huoxue Decoction
Endoplasmic reticulum stress
DUSP1
NDUFS4
Mitochondrial metabolic reprogramming

ABSTRACT

Zishen Huoxue (ZSHX) Decoction can ameliorate myocardial ischaemia by regulating the mitochondrial quality control network. However, the identification of new molecular targets is necessary for ZSHX's control of mitochondrial protein homeostasis and metabolic activities. Utilizing animal and cellular models with NDUFS4^{CKO} or DUSP1^{CKO}, along with single-cell sequencing, metabolomics, network pharmacology, and *in vivo*/*in vitro* interventions, the study found that ischemia-reperfusion (I/R) injury triggers endoplasmic reticulum stress and mitochondrial metabolic reprogramming, accompanied by downregulation of DUSP1 and NDUFS4. Network pharmacology suggested ZSHX's role in regulating mitochondrial activity during inflammatory damage, while metabolomics confirmed that ZSHX alters metabolite composition and expression in I/R-affected tissues. Single-cell sequencing further linked I/R to disrupted mitochondrial energy metabolism and cell death, and *in vitro* experiments demonstrated that ZSHX preserves mitochondrial proteostasis, inhibits endoplasmic reticulum stress, restores calcium balance, upregulates DUSP1/NDUFS4 expression, and controls metabolic reprogramming to reduce myocardial inflammatory injury. Kaempferol, the primary active component of ZSHX, drives these protective effects by enhancing DUSP1/NDUFS4 expression, thereby preventing endoplasmic reticulum stress and inflammatory bursts, preserving mitochondrial function, and re-encoding mitochondrial metabolic processes post-I/R injury.

1. Introduction

Ischemic cardiomyopathy is a condition resulting from a persistent imbalance between the heart's oxygen supply and demand, leading to myocardial cell death, fibrotic scarring, and progressive ventricular dysfunction [1]. The disease typically manifests several years after the initial segmental loss of functional myocardial tissue and is characterized by multiple discrete foci of injury within the ventricular wall. The surrounding non-infarcted myocardium compensates for the lost contractile function, although it cannot fully restore myocardial mass or performance. ischemic cardiomyopathy is hypothesized to involve chronic activation of the immune system. As adverse ventricular remodelling progresses, macrophages and T cells become pathologically activated, and elevated levels of proinflammatory cytokines contribute to ongoing cardiac injury. Persistent immune activation is thought to reflect dysregulation of immunological homeostasis. Therefore, suppression of the inflammatory response represents a key strategy for limiting peripheral tissue damage [2]. While current pharmacological and interventional therapies effectively reduce ischemic burden and improve symptom control and quality of life, none have demonstrated a definitive prognostic benefit [3]. Thus, elucidating the mechanisms underlying sustained inflammatory activation in ischemic cardiomyopathy is essential for the development of novel therapeutic approaches.

Mitochondrial dysfunction is a central driver of pathological mechanisms in ischemic cardiomyopathy [4, 5]. During ischemia or hypoxia, mitochondrial reactive oxygen species (ROS) disrupt mitochondrial dynamics, leading to DNA damage and impaired mitochondrial protein homeostasis [6, 7]. The mitochondrial proteome is highly dynamic, capable of adjusting organelle function to meet cellular energy demands. Defects in protein homeostasis result in proteotoxic stress and ultimately trigger cell death. The endoplasmic reticulum (ER), an intracellular organelle, plays a critical role in facilitating proper protein folding [8]. When misfolded proteins accumulate, ER function is compromised, leading to ER stress [9]. To restore ER homeostasis, the adaptive unfolded protein response (UPR) is activated [10]. However, prolonged or excessive ER stress leads to a maladaptive UPR, which promotes apoptotic cell death. Although ER stress has been reported in ischemic cardiomyopathy, the upstream regulatory mechanisms remain poorly understood.

Mutations in mitochondrial proteins can induce mitochondrial metabolic reprogramming to balance cellular bioenergy supply with metabolic demand. Metabolic signals regulate various mitochondrial processes, including dynamics and turnover. Inhibition of oxidative phosphorylation (OXPHOS) is generally associated

* Corresponding author.
E-mail addresses: liuruxiu1@163.com (R. Liu); xingchang_tcm@outlook.com (X. Chang)
Δ These authors contributed equally to this work.

https://doi.org/10.1016/S1875-5364(26)61171-5

with increased mitochondrial fission, whereas enhanced OXPHOS activity promotes mitochondrial fusion [11]. Elevated mitochondrial phagocytosis is also observed under metabolic conditions that support increased mitochondrial activity. The growth-associated mTORC1 pathway is inhibited by AMPK activation, which phosphorylates ULK1 and ULK2 to initiate mitochondrial autophagy [11]. OXPHOS regulation and evasion of apoptosis may be coordinated through shared molecular mechanisms. The glucose-sensing BAD protein, a member of the BH3-only pro-apoptotic family, is activated *via* phosphorylation during glucose deprivation, thereby inducing apoptosis. Additional stimuli for BH3 protein activation include low cellular energy states, while upregulation of energy metabolic fluxes can suppress pro-apoptotic signals [12]. Targeting mitochondrial metabolic reprogramming offers therapeutic potential in cancer, haematological disorders, and immune diseases by enabling the generation of new cellular phenotypes [12, 13]. The extent of cardiac functional recovery depends on the regenerative reserve of the non-ischemic myocardium, which is largely determined by cellular processes that enhance the volume of viable tissue [1]. Novel treatment strategies for ischemic cardiomyopathy could therefore involve metabolic reprogramming to stimulate sufficient cardiomyocyte proliferation for replacing damaged cells. However, identifying new molecular targets is required to enable such interventions.

DUSP1 encodes a dual-specificity phosphatase that dephosphorylates both tyrosine and threonine residues. DUSP1 expression is downregulated following acute myocardial ischemic injury [14]. By inhibiting the c-Jun N-terminal kinase (JNK) pathway, DUSP1 attenuates mitochondrial fission and autophagy, thereby reducing myocardial ischemia-reperfusion (I/R) injury (MIRI) [15]. DUSP1-mediated inactivation of JNK and the p38 pathway also dampens the inflammatory response and limits neutrophil infiltration. DUSP1 is known to regulate key aspects of mitochondrial biology, prompting us to investigate whether it also modulates ER stress and mitochondrial metabolic reprogramming to protect against myocardial ischemic inflammatory injury. In this study, we evaluated the effect of Zishen Huoxue Decoction (ZSHX) on DUSP1 expression in ischemic cardiomyopathy and its role in mediating mitochondrial metabolic reprogramming and maintaining intrinsic proteomic homeostasis.

2. Material and methods

2.1. Preparing drugs and screening for doses

Oral gavage with ZSHX was administered at a dose of 0.34 $g \cdot kg^{-1} \cdot d^{-1}$ for the high-dose group and 0.18 $g \cdot kg^{-1} \cdot d^{-1}$ for the low-dose group. All medications were consistently supplied by the pharmacy department of Guang'anmen Hospital of China Academy of Traditional Chinese Medicine (CATCM). 3-Methyladenine (3MA) and urolithin A were purchased from commercial sources as specified. Kaempferol was administered to mice in the low-dose and high-dose groups at 10 and 20 $mg \cdot kg^{-1} \cdot d^{-1}$, respectively, as a pretreatment. Kaempferol treatment began on the second day post-modeling and continued until the day before sample collection [16]. Empagliflozin (10 $mg \cdot kg^{-1} \cdot d^{-1}$) was administered seven days prior to myocardial ischemia, in accordance with a previous study [16]. Mitochondria-derived peptide (MOTS-c) (15 $mg \cdot kg^{-1}$, Phoenix Pharmaceuticals, Inc., Cat. No.: 038-48) was delivered daily *via* intraperitoneal injection for seven days before induction of myocardial ischemia [17].

2.2. Experimental animal

$DUSP1^{f/f}$/$DUSP1^{CKO}$/$NDUFS4^{CKO}$/$NDUFS^{TG}$ mice were generated by combining previously established models with relevant genetic materials [18]. The study protocol was reviewed and approved by the Ethics Committee of Guang'anmen Hospital in accordance with the ARRIVE guidelines for animal research. Adult male C57BL/6 mice (7–8 weeks old) were housed at the Animal Experiment Centre of Guang'anmen Hospital under standardized conditions. The environment was maintained at 23–25 °C with a 12-hour light/dark cycle and 55% ± 5% humidity. Mice had ad libitum access to water and standard laboratory chow for at least seven days prior to experimentation.

2.3. Myocardial I/R animal model

The mouse model of myocardial ischemic injury was established using coronary ligation techniques, as previously described [19]. Experimental animals were anesthetized *via* intraperitoneal injection of pentobarbital (50 $mg \cdot kg^{-1}$). The depth of anesthesia was confirmed by the absence of a withdrawal reflex when the hind limbs were gently clamped with non-invasive hemostatic forceps. After surgical site preparation, animals were secured on a thermostatically controlled operating table to maintain core body temperature at 35–37 °C. The left thoracic wall was accessed *via* blunt dissection between the third and fourth intercostal spaces. The thoracic cavity was opened, the pericardium was incised, the heart was gently exteriorized, and the left anterior descending artery (LAD) was ligated 1–2 mm from its origin (between the left auricle and pulmonary trunk) using a 6–0 sterile silk suture with a slip-knot technique. Successful occlusion was confirmed by immediate pallor of the left ventricular apex. The chest was then closed in layers, and thoracic decompression was performed to prevent pneumothorax. After 30–45 min of ischemia, a second thoracotomy was performed to release the ligature and restore coronary flow, thereby establishing the I/R model. Sham-operated animals underwent identical procedures without vessel occlusion. Postoperatively, penicillin G (18 000 $U \cdot kg^{-1}$) was administered intramuscularly for three consecutive days to prevent infection. To delineate the area at risk (AR), Evans blue dye was injected intravenously after re-ligation of the LAD. Following heart excision, horizontal sections were prepared. Normally perfused myocardium stained blue, whereas the ischemic region remained unstained. After removal of the right ventricular wall, the non-ischemic (blue) and ischemic (unstained) regions were separated along the demarcation line. The infarct area was calculated as a percentage of the AR, and the AR was expressed as a percentage of the left ventricle (LV). These parameters served as key indices for model validation and intervention assessment [20, 21]. Additionally, echocardiographic parameters, including left ventricular ejection fraction (LVEF), left ventricular fractional shortening (LVFS), left ventricular septal end-diastolic thickness (LVSd), and early to late diastolic flow velocity ratio (E/A ratio), were measured to evaluate systolic function, myocardial structure, and diastolic function post-modeling.

2.4. Grouping animals and intervening

Animals were assigned to the following groups: (1) Sham group, (2) I/R group, (3) I/R + ZSHX-High group, (4) I/R + ZSHX-Low group, (5) I/R + Empagliflozin group, (6) I/R + Mots-c group, (7) I/R + KAE group, (8) I/R + KAE + $NDUFS4^{CKO}$ group, and (9) I/R + KAE + $DUSP1^{CKO}$ group. Drug administration commenced on the second day after successful model establishment. ZSHX (high and low doses) was administered to the respective treatment groups. The positive control, empagliflozin (10 $mg \cdot kg^{-1} \cdot d^{-1}$), was administered eight weeks prior to myocardial infarction (MI) modeling [22]. Mots-c (15 $mg \cdot kg^{-1}$) was administered intraperitoneally as described in the reference study [17]. The treatment duration was eight weeks.

2.5. Cardiomyocyte culture

Cardiomyocytes were isolated from wild-type (WT), DUSP1^{CKO}, and NDUFS4$^{TG/CKO}$ mice for *in vitro* experiments. Hearts from neonatal mice were collected and subjected to sequential enzymatic digestion to isolate cardiomyocytes, which were identified by spontaneous contractile activity. Primary cardiomyocytes were cultured in an incubator maintained at 37 °C with 5% CO_2.

2.6. Cell grouping and intervention

In vitro, si-DUSP1/ad-DUSP1 and si-NDUFS4/ad-NDUFS4 constructs were generated *via* adenoviral transfection. The following groups were established: (1) Ctrl group; (2) I/R group; (3) I/R + ZSHX-Hi group; (4) I/R + ZSHX-Low group; (5) I/R + ZSHX + si-DUSP1 group; (6) I/R + ZSHX + ad-DUSP1 group; (7) I/R + KAE group; (8) I/R + KAE + 3MA group; (9) I/R + KAE + Urolithin A group; (10) I/R + KAE + NDUFS4^{TG} + si-DUSP1 group; (11) I/R + KAE + NDUFS4^{TG} + ad-DUSP1 group; (12) I/R + KAE + Mots-c group; (13) I/R + KAE + mitochondrial oxidative phosphorylation uncoupler (FCCP) group; (14) I/R + KAE + NDUFS4^{CKO} + si-DUSP1 group; (15) I/R + KAE + NDUFS4^{CKO} + ad-DUSP1 group; (16) I/R + ZSHX + si-NDUFS4 group; (17) I/R + ZSHX + ad-NDUFS4 group. Cells were pretreated with kaempferol for 48 h prior to modeling. As per established protocols, cardiomyocytes were pretreated with ZSHX at concentrations of 100 and 400 μg·mL^{-1}. To induce mitophagy, FCCP (5 μmol·L^{-1}) was applied for 120 min. To inhibit mitophagy, 3-MA (10 mmol·L^{-1}) was administered for 2 h [14, 23].

2.7. Immunofluorescence assay

Cells were fixed at room temperature after washing with PBS. After blocking with 5% goat serum for 30 min, primary antibodies were added and incubated overnight at 4 °C. Following three washes, fluorescent secondary antibodies were applied at 37 °C for 30 min. After additional washes, nuclei were stained with DAPI for 10 min, and coverslips were mounted for imaging.

2.8. Enzyme-linked immunosorbent assay (ELISA)

Serum was collected from each batch of mice by cardiac puncture and centrifuged for storage. Levels of tumor necrosis factor α (TNF-α) and interleukin-6 (IL-6) were measured using commercial ELISA kits according to the manufacturer's instructions. Concentrations in each group were determined using standard curves based on absorbance readings.

2.9. Western blot (WB) assay

Proteins were extracted from cells in each group and quantified. Equal amounts of protein were loaded onto SDS-PAGE gels for electrophoresis, followed by transfer to PVDF membranes. Membranes were blocked with 5% skim milk for 1 h at room temperature. Primary antibodies were incubated overnight at 4 °C, followed by secondary antibodies for 90 min at room temperature. After three washes, membranes were developed using ECL chemiluminescent substrate.

2.10. Real-time polymerase chain reaction (RT-PCR)

Total ribonucleic acid (RNA) was extracted from each cell group using the Trizol method, and RNA concentration was determined. cDNA was synthesized *via* reverse transcription. RT-PCR was performed using the SYBR® Premix Ex Taq™ II system according to the manufacturer's protocol. The Ct values were recorded, with *β*-actin used as the internal reference. Relative gene expression was calculated using the $2^{-\Delta\Delta Ct}$ method.

2.11. Metabolomics

For metabolomic analysis, 60 mg of sample and 600 μL of methanol (V:V = 4:1, containing mixed internal standard, 4 μg·mL^{-1}) were added to a 1.5 mL centrifuge tube. The mixture was pre-cooled at −40 °C for 2 min, then ground at 60 Hz for 2 min. Subsequently, ultrasonic extraction was performed in an ice-water bath for 10 min, followed by incubation at −40 °C overnight. Samples were centrifuged at 12 000 r·min^{-1} for 10 min at 4 °C. A 150 μL aliquot of supernatant was collected using a syringe, filtered through a 0.22 μm organic-phase syringe filter, transferred to an LC vial, and stored at −80 °C until liquid chromatography-mass spectrometry (LC-MS) analysis. Equal volumes of all extracts were pooled to generate quality control (QC) samples (all reagents were pre-cooled at −20 °C before use). Analysis was performed using a liquid chromatography–mass spectrometry system consisting of a Waters ACQUITY UPLC I-Class plus coupled to a Thermo QE Plus ultra-high-performance liquid tandem high-resolution mass spectrometer. System stability and sample preparation consistency were monitored using internal standards and QC samples throughout the analytical run.

2.12. Network pharmacology

Active compounds of ZSHX were identified by querying the TCMSP database (http://tcmspw. com/tcmsp.php). Disease-related targets associated with "myocardial infarction" were retrieved from DrugBank (https://go.drugbank.com/), GeneCards (https://previous.genecards.org/), and OMIM (https://previous.genecards.org/) databases.

Overlapping targets between ZSHX and MI were identified using Venny 2.1.0 to generate Venn diagrams. A protein–protein interaction (PPI) network was constructed using the STRING database (https://cn.string-db.org/) and visualized in Cytoscape software. Gene Ontology (GO) functional enrichment and Kyoto Encyclopedia of Genes and Genomes (KEGG) pathway analyses were subsequently performed.

2.13. Molecular docking

Mouse target proteins MLKL (PDB ID: 4BTF), NDUFS4 (PDB ID: 6G2J), RIPK3 (PDB ID: 6OKO), activating transcription factor 6 (ATF6), and DUSP1 were retrieved from the PDB database (https://www1.rcsb.org/). For ATF6 and DUSP1, which lack experimentally resolved structures, predicted three-dimensional (3D) models were obtained from AlphaFold based on high sequence homology. The ligand kaempferol was downloaded from the PubChem database. The 3D conformation of kaempferol was energy-minimized using Chem3D (version 2020) with molecular mechanics to obtain the lowest-energy conformation for docking simulations.

2.14. Single-cell sequencing

Single-cell transcriptomic datasets from the GEO database (GSE270961 and GSE163956) were analyzed, including left ventricular (LV) samples from sham-operated controls (normal control, n = 2) and acute MI (AMI) mice (within one week post-MI, n = 3). Mitochondrial-related genes were obtained from the MitoCarta3.0 database. Mitochondrial-associated differentially expressed genes (MitoDEGs) were identified by intersecting DEGs from control and AMI groups with mitochondrial genes. Raw data were preprocessed using the Seurat package (v4.4.0) in R. The "PercentageFeatureSet" function was used to calculate mitochondrial and ribosomal RNA content. Only cells expressing 300–7000 genes with less than 20% mitochondrial reads were retained. Cells with RNA counts below the 97th percentile were excluded, while those with over 1000 RNA counts were included. Data were log-normalized, and highly variable genes were identi-

fied using "FindVariableFeatures" and scaled using principal component analysis (PCA). Cell clustering was performed using the "FindNeighbors" and "FindClusters" functions (resolution = 0.1) within the Uniform Manifold Approximation and Projection (UMAP) dimensionality reduction framework. Marker genes for each cluster were identified using the "FindAllMarkers" function (adjusted *P*-value < 0.05). Cell identities were annotated by cross-referencing marker genes with the PanglaoDB database (https://panglaodb.se) and the "singleR" package. Gene set variation analysis (GSVA, v1.48) was used to assess gene set expression across cell types. Gene set enrichment analysis (GSEA) was conducted using the "clusterProfiler" package (v4.2.2), with gene sets derived from the "M5" collection of the Molecular Signatures Database (https://www.gsea-msigdb.org/gsea/msigdb/index.jsp).

2.15. Statistical methods

Data are presented as mean ± standard error. For comparisons between two groups, the t-test was used; for multiple groups, one-way ANOVA was applied. All data were analyzed using GraphPad Prism 9 software. Statistical significance was defined as $P < 0.05$.

3. Results

3.1. Single-cell RNA sequencing analyses mitochondrial energy metabolism and cell death pathways

Following data quality assessment (Fig. 1A), gene expression matrices underwent Harmony-based batch effect correction (Fig. 1B), and the top ten highly variable genes are displayed (Fig. 1C). To determine the optimal resolution for unsupervised clustering, we evaluated 10 different resolution parameters (Fig. 1D). A resolution of 0.1 was selected to accurately distinguish cell types based on predefined annotations. UMAP identified 9 distinct cell clusters, each labeled with a unique color (Fig. 1E). By integrating gene expression profiles with CellMarker annotations, we refined the UMAP clustering to identify eight cell types: fibroblasts, macrophages, endothelial cells, oligodendrocytes, B cells, neutrophils, enterocytes, and smooth muscle cells (Fig. 1F). A heatmap showed pairwise expression comparisons across cell types (Fig. 2A). We identified 2662 DEGs ($\log_{10}$ FC > 1, adjusted *P*-value < 0.05) between the AMI and NC groups using the "FindMarkers" function. These were intersected with a mitochondrial gene set to yield 552 MitoDEGs. A dot plot illustrated the average log2 fold change of key genes (Fig. 2B). GSVA was applied across the 8 cell types, with enrichment scores linked to pathways such as cell chemotaxis and vascular endothelial growth factor signaling (Fig. 2C). Cardiac troponin T (TnT) proteins—encoded by TNNT1, TNNT2, and TNNI3—are highly sensitive and specific biomarkers of myocardial injury, with TNNT2 being the predominant isoform. Our results confirmed higher expression of TNNT2 compared to TNNT1, particularly in fibroblasts and macrophages, in both the AMI and NC groups (Figs. 2D and 2E). GSEA analysis highlighted processes including regulation of proteolysis, cytochrome c release, and programmed cell death (Fig. 2F). Additional volcano plots illustrated the distribution of MitoDEGs in the disease context and within fibroblast and macrophage subpopulations (Figs. 2G and 2H), evealing four overlapping genes: *Adhfel*, *Abcd2*, *AA467197*, and *Nt5dc2* (Fig. 2I).

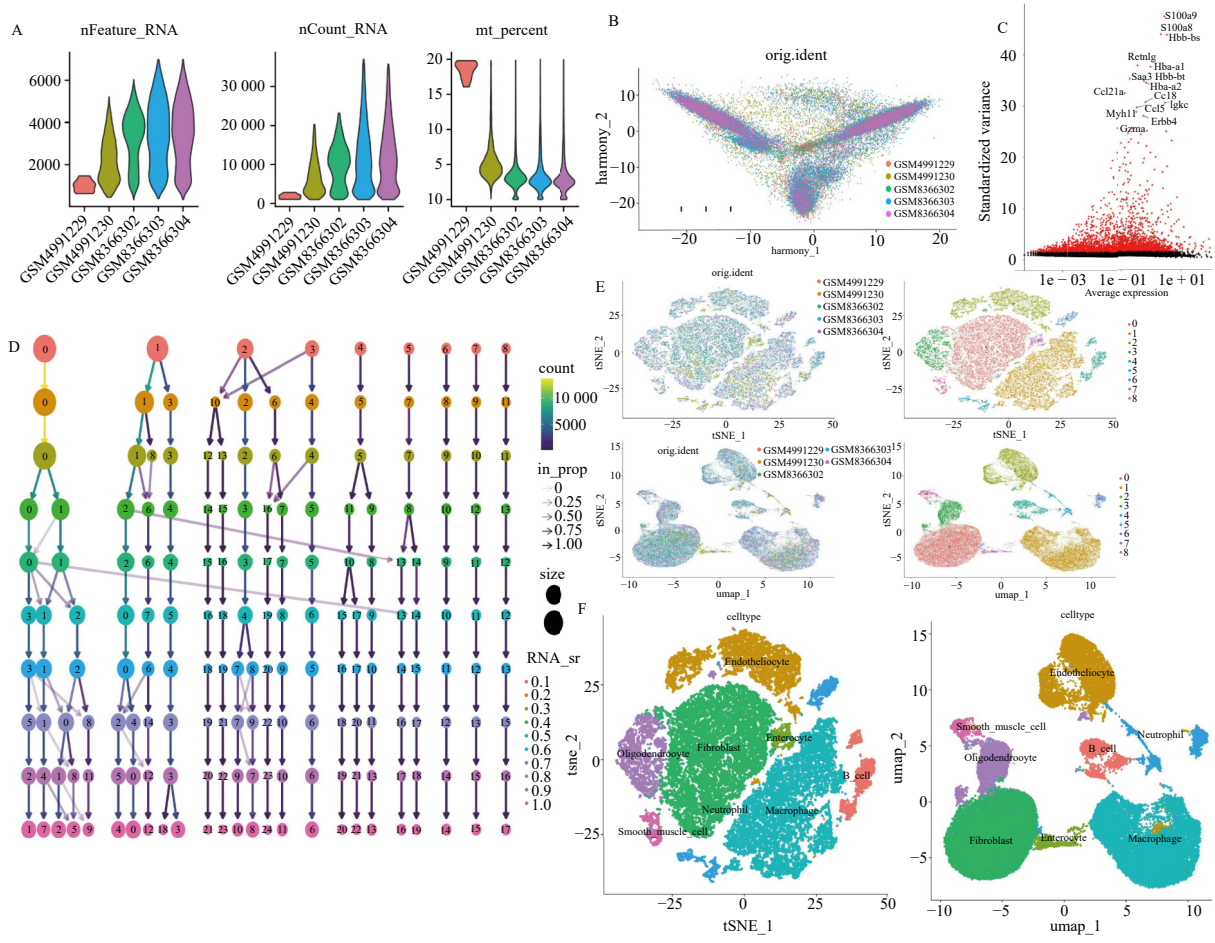

Fig. 1 (A) RNA-seq data quality control violin plot. (B) PCA clustering plot after Harmony. (C) highly variable genes. (D) clustering tree plot using principal components. (PCs) to determine the degree of separation. (E) Unified Flow Approximation and Projection Clustering for 9 clusters. (F) UMAP plot after performing cellular annotation.

3.2. ZSHX suppresses I/R-induced myocardial inflammation and ER stress

The WB results showed that compared to the sham group, the expression of DUSP1 and NDUFS4 in the I/R group was reduced (Figs. 3A–3C). The immunofluorescence experiment revealed that Gr-1/TnT fluorescence intensity increased during I/R injury, implying that I/R caused myocardial inflammatory injury (Fig. 3D). The echocardiography results in mice indicated that the I/R group exhibited impaired cardiac function, including decreased systolic function (lower LVEF and LVFS), altered myocardial structure (thickened LVSd), and diastolic dysfunction (reduced E/A Ratio) (Figs. 3E and 3F). In contrast, the high-dose ZSHX group significantly improved the decline in cardiac function, similar to the effects of MOTS-c and EMPA (Figs. 3D–3F). The ELISA assay showed that the I/R group had considerably higher levels of inflammatory factors including TNF-α/IL17/IL18. Low concentrations of ZSHX party intervention did not significantly reduce inflammatory factor levels. High concentrations of ZSHX intervention not only improved infarct size but also dramatically reduced Gr-1/TNF-α/IL17/IL18 levels (Figs. 3E, Supplementary Figs. 1A and 1B).

The I/R group showed an increase in ATF-6/PERK/CHOP transcription, which was reversed by a high dosage of ZSHX (Supplementary Fig. 1C). ZSHX party intervention increased the expression of the mitochondrial inner membrane protein PHB2 (Supplementary Fig. 1D). Using Empagliflozin and MOTS-C as positive medications, the comparison demonstrated that ZSHX's efficacy in inflammation and ER stress inhibition was comparable to the positive pharmaceuticals, with no statistically signific-

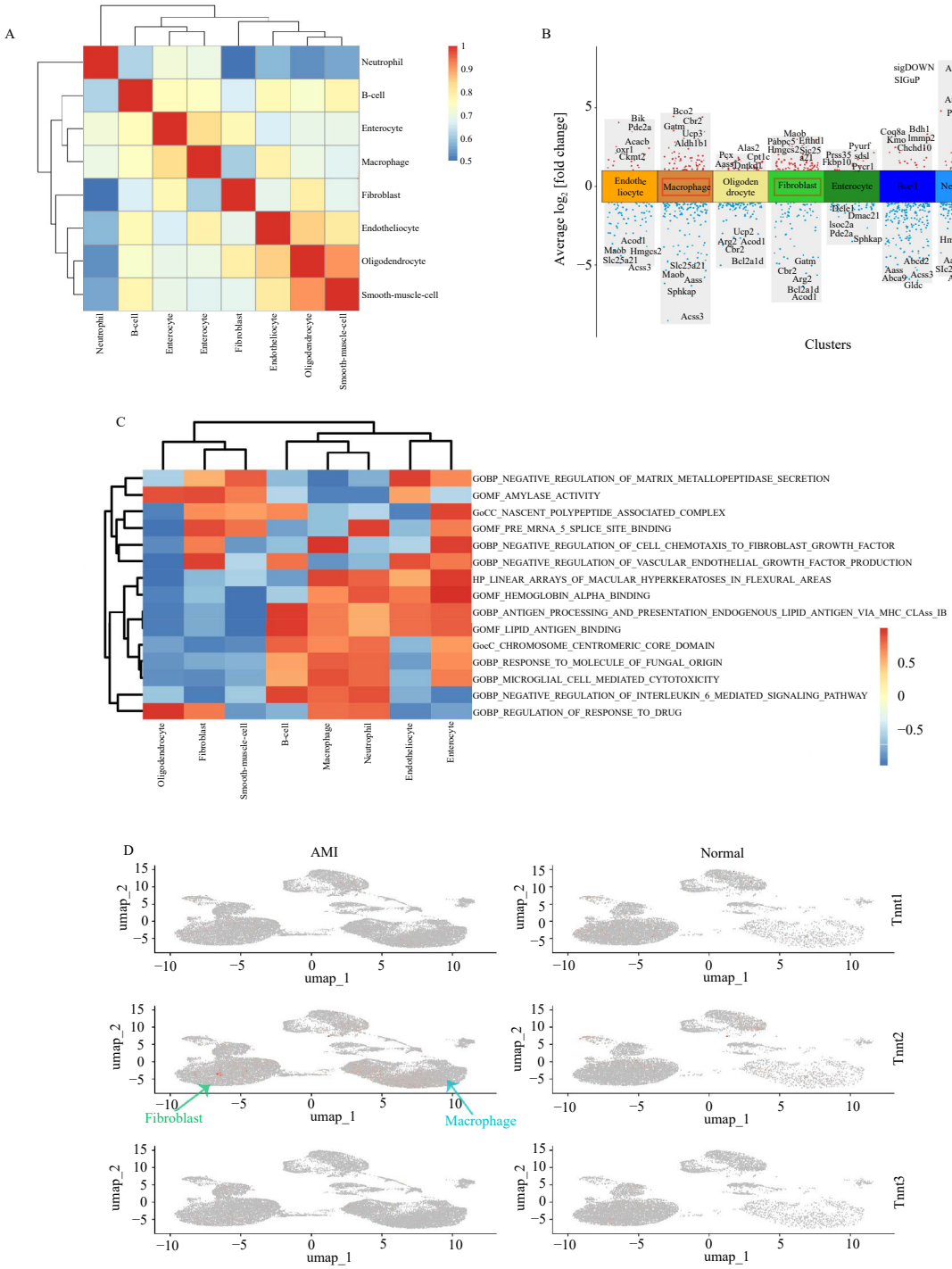

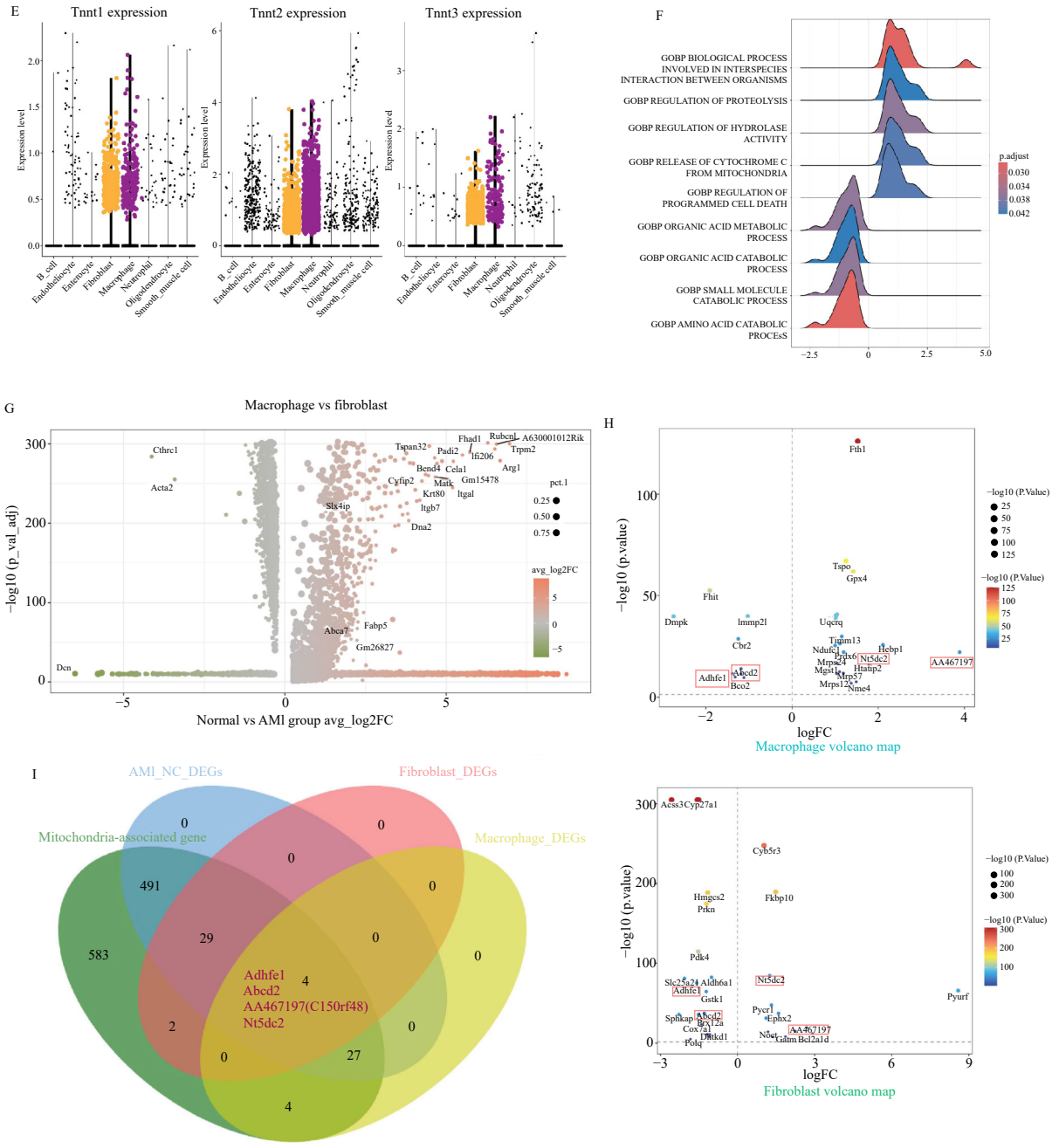

Fig. 2 (A) Correlation heatmap of 8 cell types. (B) Expression of mitochondria-associated differential gene (MitoDEG) in 8 cell types. (C) GSVA analysis of scores of different cell types. (D) Characteristic plots showing the expression patterns of TNNT1, TNNT2, and TNNI3 in LV cells of the AMI group and the control group. (E) Violin plots showing the expression of TNNT1, TNNT2, and TNNI3 in eight cell types. (F) Ridge plot showing GSEA analysis of MitoDEG. (G) Volcano plot of MitoDEG expression in AMI and normal control (NC) groups. (H) Volcano plot of MITODEG expression in fibroblasts and macrophages. (I) Wayne plot of line body-associated gene-differential gene-fibroblast-macrophage intersection.

ant difference between the three groups (Supplementary Figs. 1B–1D). To determine the major active constituents of ZSHX, we analysed the herbal components using high performance liquid chromatography (HPLC). The results revealed that the ZSHX sample comprised mostly seven peaks with good peak symmetry. Following comparison and analysis with standard profiles, seven useful substances were identified: liquiritin, notoginsenoside R1, quercetin, Gginsenoside Rb1, kaempferol, astragaloside A, and tanshinone IIA (Supplementary Fig. 1E).

3.3. Network pharmacology in conjunction with metabolomics data validates that DUSP1 impacts the metabolic pathway of fat and other substances and participates in apoptotic processes

The Western Blot assay demonstrated that DUSP1 and NDUFS4 protein expression was reduced after I/R injury, but ZSHX increased DUSP1 and NDUFS4 expression in I/R injured myocardium (Figs. 4A–4C). Network pharmacology revealed that ZSHX and MIRI co-targeted 139 genes (Supplementary Fig. 2A) and identified the key genes *TNF*, *AKT1*, *IL6*, *IL1B*, *BCL2*, *CASP3*, *TP53*, and *STAT3*.The co-intersecting targets were subjected to the PPI protein interactions network design to yield the major targets Bax, Casp, NFKBIA, and Bcl2 (Supplementary Figs. 2B and 2C).

At the same time, the intersecting targets were subjected to GO and KEGG pathway analysis, and it was clear that the target genes were related to mitochondrial structure and apoptotic complex synthesis, which influenced the pathways of inflammatory response, DNA regulation, and apoptosis (Supplementary Fig. 2D). ZSHX impacted TNF-α/IL-6/IL-10/IL-1β/Bax/Bcl-2/Cas-

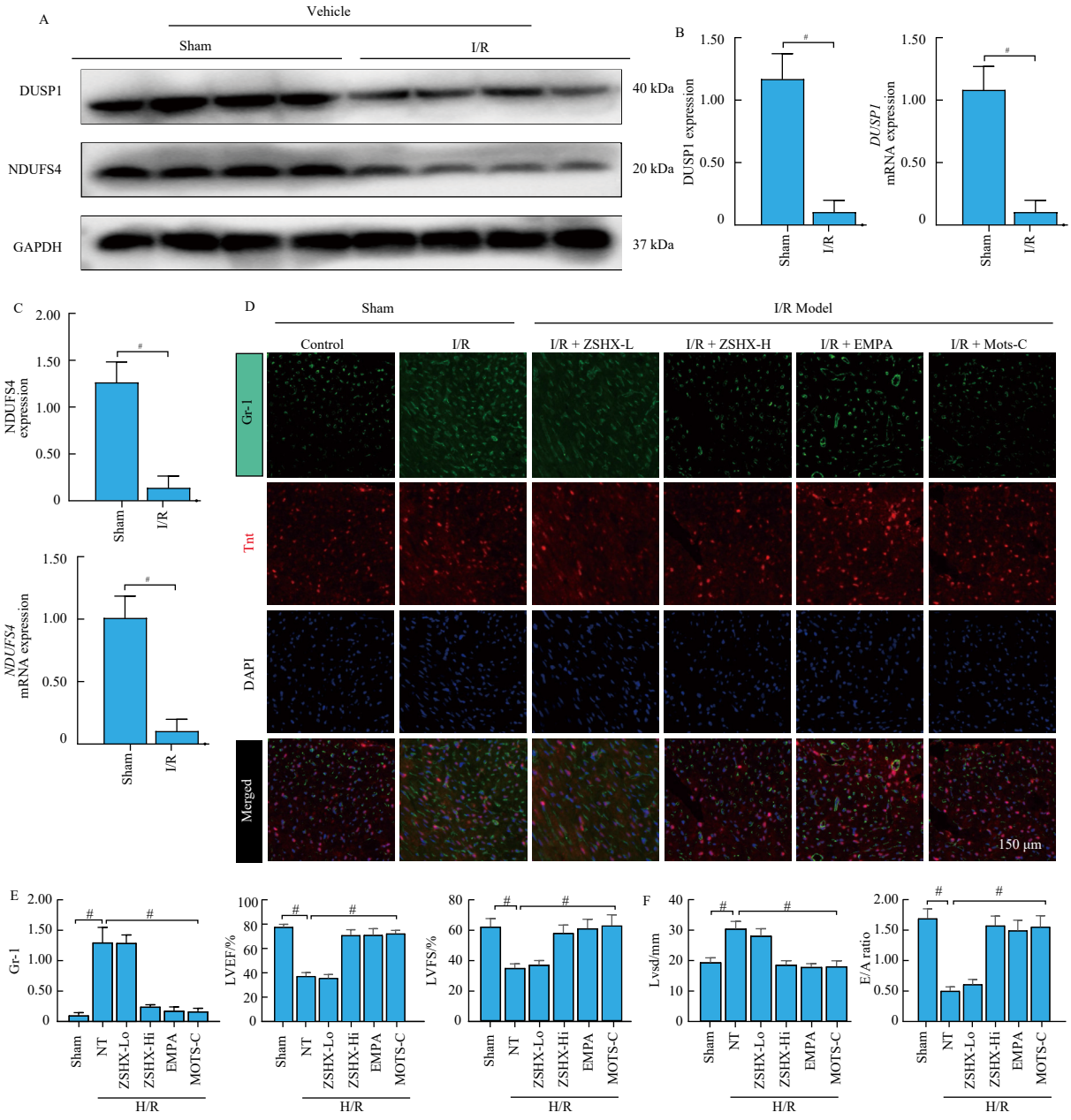

Fig. 3 (A) WB detection of DUSP1/NDUFS4 protein. (B) Transcription and protein expression of DUSP1. (C) Transcription and protein expression of NDUFS4. (D) Immunofluorescence of Gr-1/Tnt. (E, F) The assessment of cardiac ultrasound function in mice [LVEF (left ventricular ejection fraction), LVFS (left ventricular shortening fraction), LVSd (interventricular septal thickness at end-diastole), E/A ratio (ratio of early to late diastolic flow velocity)]. Elisa detection of Gr-1. Data are expressed as mean ± SD (n = 8 mice/group). For panels B and C, statistical significance was analyzed using an unpaired two-tailed Student's t-test. For panels E and F, one-way ANOVA followed by Tukey's post hoc test was used. $^{\#}P < 0.05$ for the indicated comparisons.

pase levels in group I/R (Fig. 4D and Supplementary Fig. 3A). To investigate the mechanism of ischaemic cardiomyopathy and identify metabolic targets, we used metabolomics to assess metabolic indicators as the disease progressed. The findings revealed that metabolite composition was altered following I/R damage as well as ZSHX intervention therapy, with substantial changes in sample metabolite expression between groups (Supplementary Fig. 3B). Comparison of the mod and con groups showed that anandamide, MG, 3α-hydroxy-15-oxo-5b-β-chol-8-en-24-oic-acid, α-tocotrienol, 11-methoxy-octadecanoic acid, MG, lexacalcitol, nutriacholic acid, 3α-hydroxy-12-oxo-5-β-cholan-24-oic acid, cis-epsilon-octenoic acid, 16-hydroxy stearic acid and other metabolites content were significantly different (Supplementary Fig. 3B and Figs. 5A and 5B).

The levels of diferuloyputrescine, quinaprilat, 7α,12α-dihydroxy-5β-chol-2en-24-oic acid, and ethyl 16-hydroxy-18-bromo- were compared between the ZSHX and model groups, with significant density changes observed. Notably, 8*E*,17*E*,19*Z*-tricosatrien-4,6-diynoate, palmitic acid, MG, 3α-hydroxy-15-oxo-5β-chol-8-en-24-oic acid, quinaprilat, 6-β-hydroxydexamethasone, and PC (O-14:0/18:3 (9*Z*,12*Z*,15*Z*), Delta-Tha) exhibited significant alterations (Figs. 5C and 5D). Wayne and volcano plots revealed substantial differences in metabolite expression and species distribution across samples, while the heatmap highlighted specific differential metabolites (Figs. 5E and 5H, Supplementary Fig. 7).

Bar graphs illustrated the top 20 differential metabolites with the highest VIP values in the control and GT groups, along with the degree of linear CORRELATION among these metabolites (Figs 5F–5G). Functional clustering of differential metabolites in these groups revealed enrichment in tyrosine metabolism, folate biosynthesis, carbohydrate digestion and lysine degradation, ABC transporters, tryptophan metabolism, aspartate, alanine, and glutamate metabolism, caffeine metabolism, and neuro-

active ligand-receptor interactions, as determined by GSEA enrichment analysis (Figs. 6A–6C). The heatmap displayed the abundance of specific metabolites across different samples from the control and GT groups (Fig. 6B). KEGG pathway analysis indicated that differential metabolites were primarily enriched in steroid hormone biosynthesis, unsaturated fatty acid biosynthesis, arginine biosynthesis, primary bile acid biosynthesis, and the ether lipid metabolism pathway—processes implicated in cellular necroptosis and ferroptosis (Figs. 6D and 6E).

3.4. ZSHX increases DUSP1 expression, which decreases ER stress pathway-mediated mitochondrial respiratory impairment

Oxygen consumption rate (OCR) assays demonstrated that I/R injury impaired mitochondrial respiratory function and reduced adenosine 5'-triphosphate (ATP) production. ZSHX treatment enhanced mitochondrial basal respiration, maximal respiration, and the activity of Complexes I, III, and V, while also increasing ATP synthesis (Figs. 7A, 7C, 7D, 7F–7H). I/R injury reduced DUSP1 expression in cells, whereas ZSHX treatment upregulated DUSP1 in the I/R group (Figs. 7I and 7J). Following H/R insult, cell viability decreased and apoptosis increased; high-dose ZSHX restored cell viability and suppressed apoptosis, whereas si-DUSP1 abolished this protective effect (Fig. 7J). I/R injury upregulated the transcription of ER stress markers ATF6, IRE1, PERK, and CHOP, which were significantly reduced by ZSHX intervention. However, si-DUSP1 treatment prevented this suppression, and transcript levels remained elevated (Figs. 7K and 7L), The inhibitory effect of ZSHX on ER stress was dose-dependent, with limited efficacy observed at low doses. Therefore, high-dose ZSHX was selected as the optimal therapeutic dose for subsequent experiments.

In the ZSHX group, monomeric green fluorescence decreased and aggregated red fluorescence increased, indicating that I/R injury reduced mitochondrial membrane potential (Figs. 8A and 8B). High-dose ZSHX significantly improved mitochondrial energy metabolism and cellular activity. However, si-DUSP1 treatment abolished the therapeutic benefits of ZSHX, whereas ad-DUSP1 did not interfere with its efficacy (Figs. 8C–8E). Additionally, ZSHX effectively mitigated ER stress induced by injury, leading to improved protein expression and transcription levels of ATF6, IRE1, PERK, and XBP-1 (Figs. 8F–8H). DUSP1 knockdown (si-DUSP1) eliminated the targeted therapeutic effect of ZSHX, while ad-DUSP1 did not alter it (Figs. 8F–8H).

RT-PCR analysis of NDUFS4 transcription under si-DUSP1 and ad-DUSP1 conditions showed that si-DUSP1 almost completely reversed the ZSHX-induced upregulation of NDUFS4, whereas ZSHX restored NDUFS4 expression that had been suppressed by I/R injury (Fig. 8H). These findings suggest that ZSHX may regulate mitochondrial and ER homeostasis *via* the DUSP1-NDUFS4 pathway, thereby enhancing cell viability.

3.5. ZSHX overexpression of DUSP1/NDUFS4 reduces the I/R injury-induced ER stress and calcium overload

To investigate the regulatory roles of DUSP1 and NDUFS4 in

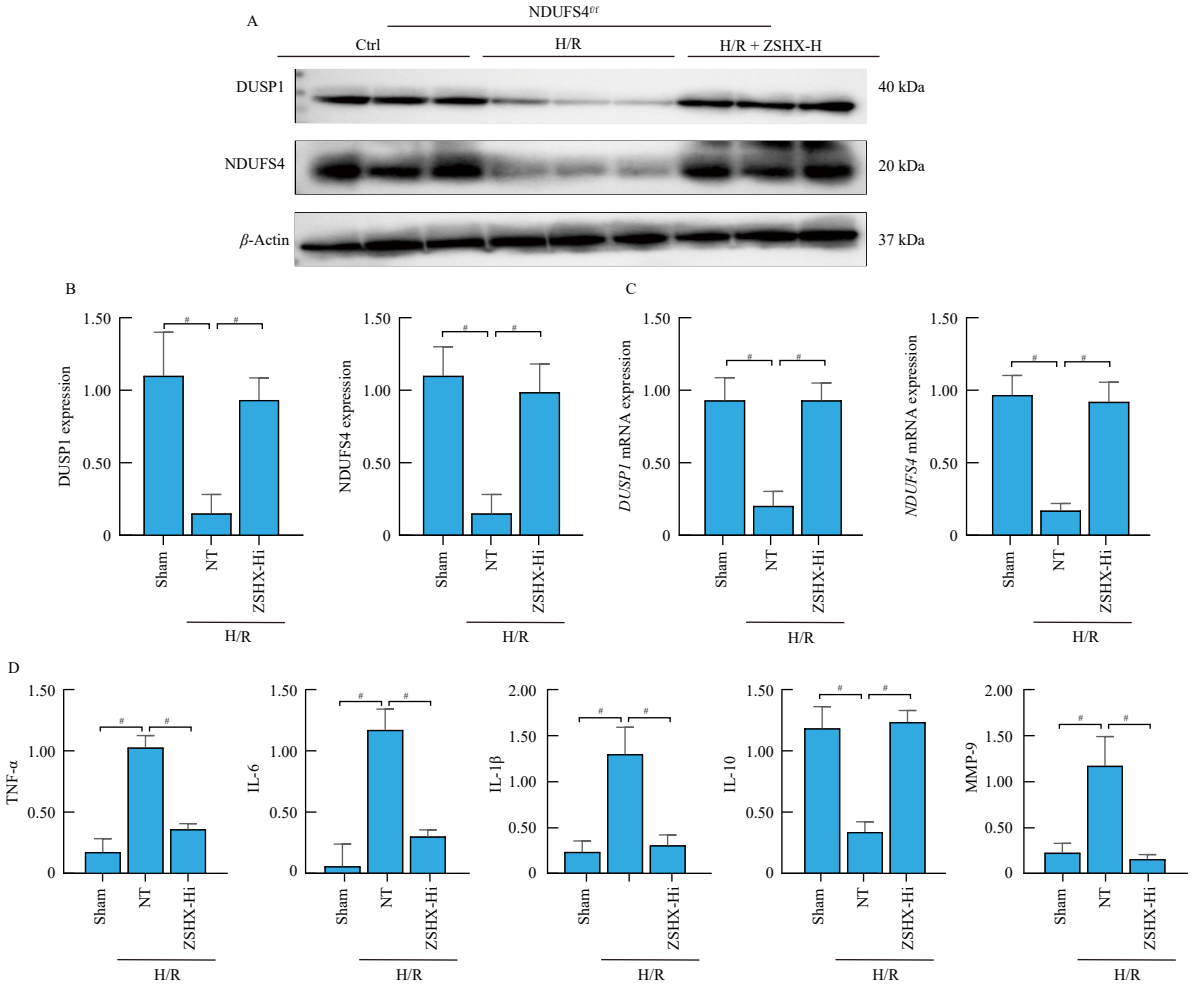

Fig. 4 (A) DUSP1 and NDUFS4 protein expression in the three groups. (B) Relative protein levels of DUSP1 and NDUFS4. (C) mRNA levels of *DUSP1/NDUFS4*. (D) Expression levels of inflammatory factors (TNF-α/IL-6/IL-10/IL-1β/MMP-9). Data are expressed as mean ± SD (n = 8 independent experiments/group). Statistical significance was analyzed using one-way ANOVA followed by Tukey's post hoc test. $^{\#}P < 0.05$ for the indicated comparisons (Ctrl *vs* H/R, and H/R *vs* H/R + ZSHX-H).

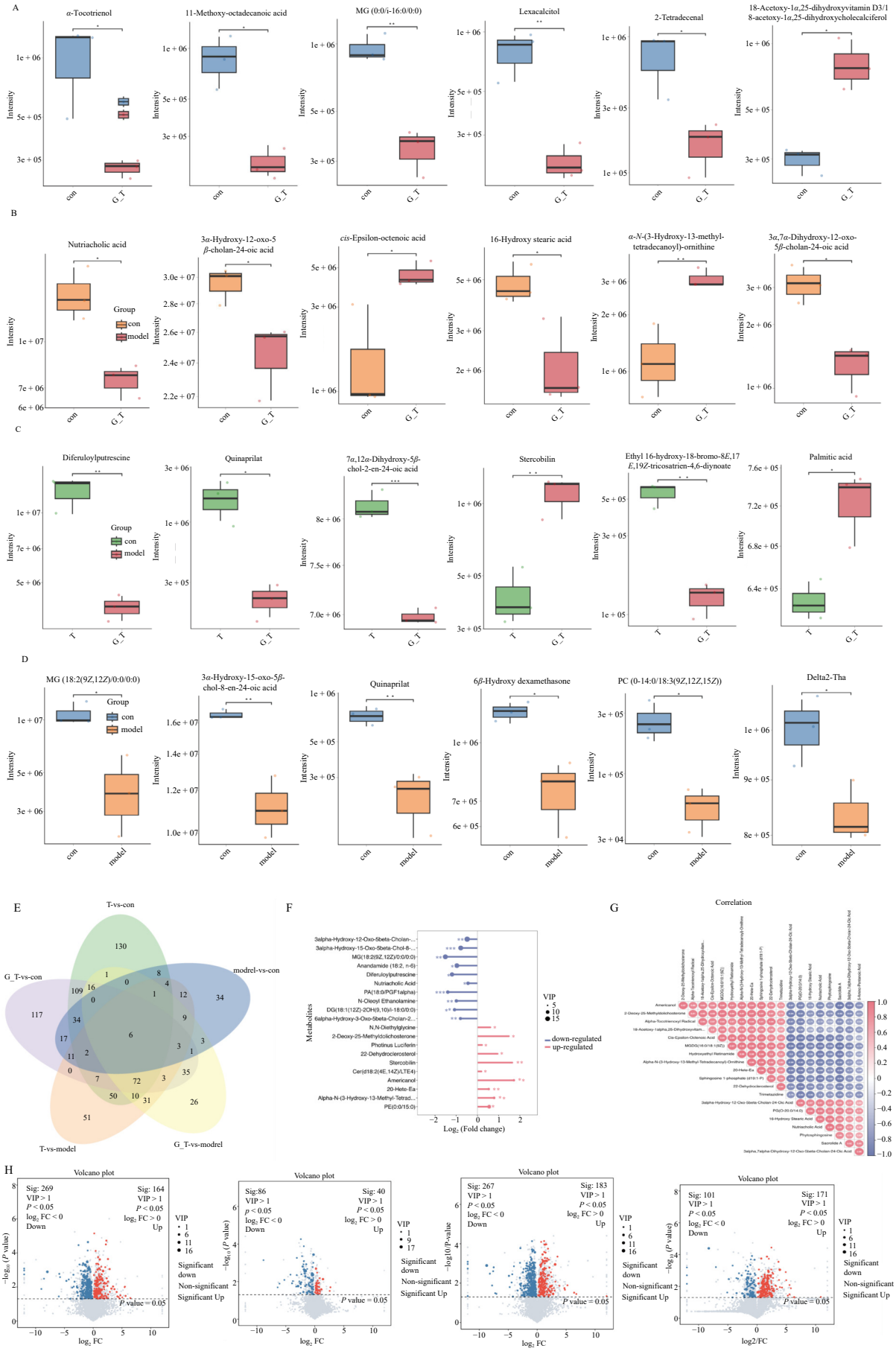

Fig. 5 (A, B) Differential metabolites between the control (Con) and model groups. (C, D) Additional comparisons of differential metabolites between the Con and model groups. (E) Venn plots showing overlap of differential metabolites among the four groups. (F) Bar plots of selected differential metabolites. (G) Correlation analysis of key metabolites (H) Volcano plot of differential metabolites.

calcium homeostasis, si-DUSP1/ad-DUSP1 and si-NDUFS4/ad-NDUFS4 cell models were generated *via* adenoviral transfection, followed by Ca^{2+} fluorescent probe labeling. Results showed that H/R injury increased intracellular Ca^{2+} concentration, whereas ZSHX improved Ca^{2+} recycling and suppressed Ca^{2+} transients. However, si-DUSP1 and si-NDUFS4 inhibited ZSHX-mediated Ca^{2+} recycling and reduced cell viability (Figs. 9A–9C). ZSHX suppressed the transcription of ER stress factors PERK, CHOP, and ATF6 by upregulating DUSP1 and NDUFS4 (Figs. 9D–9F), while promoting the expression of calcium-regulating proteins SERCA2a and Cav1.3, and suppressing RyR2 transcription, thereby modulating intracellular Ca^{2+} release and reuptake (Figs. 9G–9I). In contrast, ad-DUSP1 and ad-NDUFS4 did not further alter Ca^{2+} levels or ER stress modulation compared to the ZSHX group.

3.6. Kaempferol inhibits I/R damage and inflammatory injury by upregulating DUSP1/NDUFS4 and activating mitochondrial autophagy in the ER stress pathway

As previously established, *DUSP1/NDUFS4* gene regulate ZSHX's effects on ER function and inflammation. Based on the results of network pharmacology, to investigate the regulatory effect of kaempferol on NDUFS4 and DUSP1, we conducted the following experiments. Mice in the I/R group exhibited impaired cardiac function, while the genetically modified mice showed results highly similar to those of the I/R group even after treatment with kaempferol (Figs. 10A–10F). Conditional knockout of NDUFS4 and DUSP1 ($NDUFS4^{CKO}/DUSP1^{CKO}$) markedly blunted the suppressive effects of kaempferol on the expression of Gr-1, TNF-α, IL-17 and IL-18 (Figs. 10B, 10F, and 10G). ZSHX's major target for inflammation suppression has been confirmed as DUSP1/NDUFS4. RT-PCR was used to assess ER stress molecule mRNA transcript levels, and the results showed that $NDUFS4^{CKO}/DUSP1^{CKO}$ nearly entirely counteracted kaempferol's suppression of *ATF6/PERK/CHOP*, with transcript levels similar to those of the I/R group (Figs. 10H and 10I). RT-PCR detection of, mitophagy levels revealed that the kaempferol group significantly improved the I/R-induced low expression of PINK/Parkin/ATF5 and activated mitophagy, whereas the expression of *PINK/Parkin/ATF5* in the $NDUFS4^{CKO}/DUSP1^{CKO}$ was comparable to that of the I/R group (Figs. 10J–10L). Molecular docking confirmed that kaempferol was linked to the DUSP1/NDUFS4/ATF6/MLKL/RIPK3. Based on the predictions from network pharmacology, kaempferol exhibits a high binding affinity with core targets, which has been validated through molecular docking (Supplementary Figs. 4A–4C). Therefore, we prioritize kaempferol as a representative component for further validation of the regulatory effects of ZSHX on DUSP1/NDUFS4.

3.7. Kaempferol controls mitochondrial respiration and autophagy via DUSP1-NDUFS4

We created an I/R mouse model of $NDUFS4^{TG}$ utilising gene-modification techniques. TOM20 immunofluorescence assay revealed that 3MA inhibited mitochondrial autophagy and reduced the intensity of TOM20 red fluorescence in the ZSHX group,

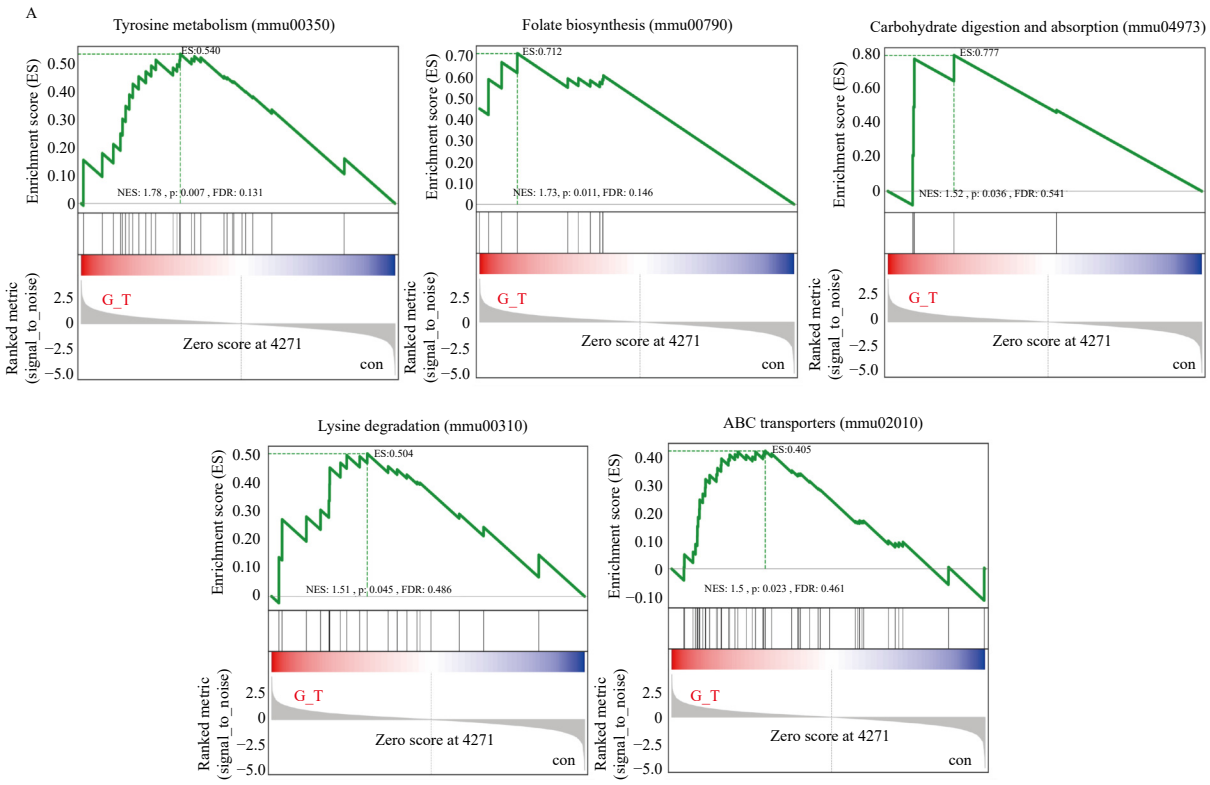

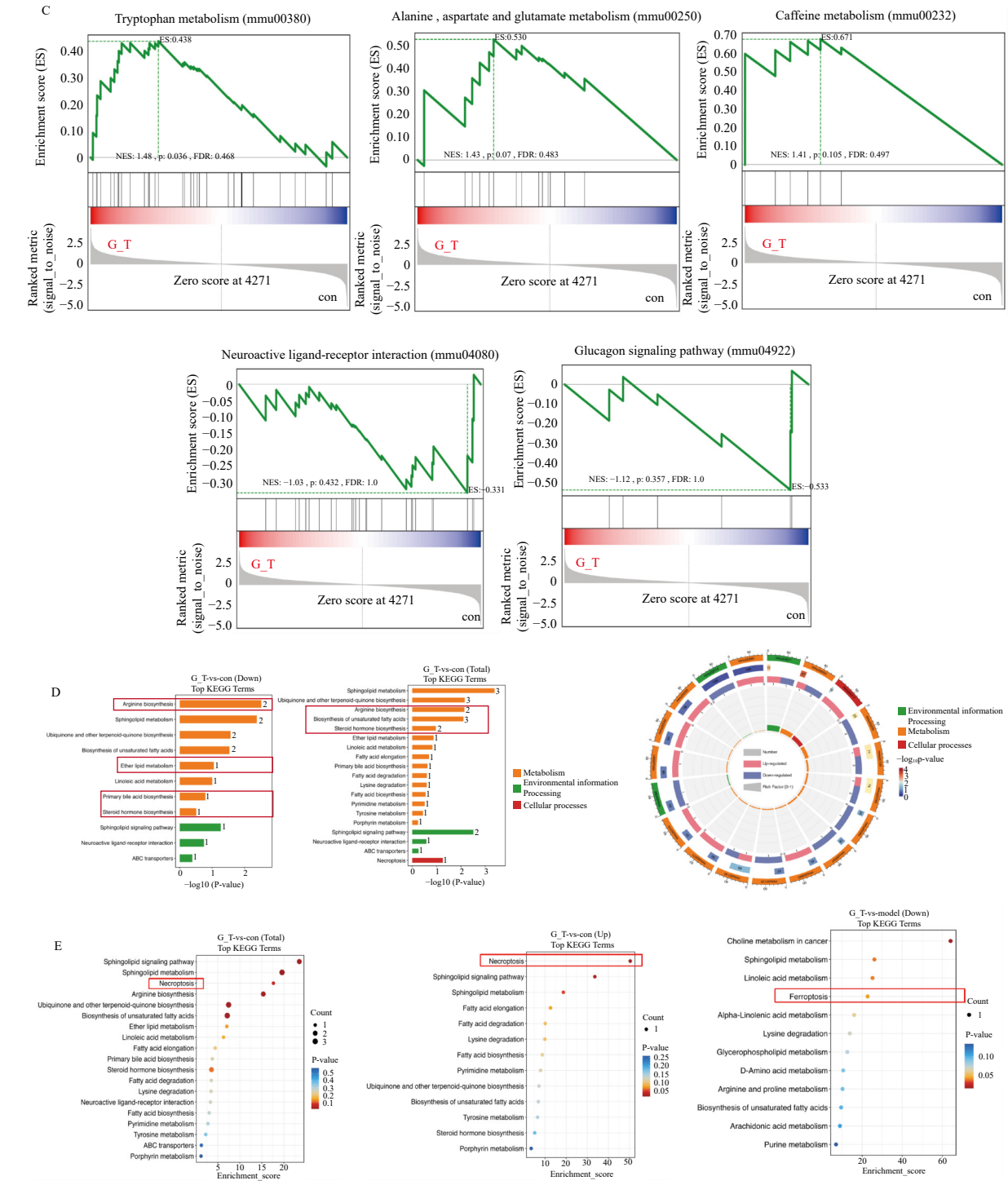

Fig. 6 (A) GSEA enrichment analysis. (B) Cluster analysis heatmap. (C) GSEA enrichment analysis. (D) KEGG enrichment bar and ring plots. (E) KEGG enrichment analysis bubble plots.

whereas urolithin A activation of mitophagy was accompanied by TOM20 cellular expression comparable to that of the ZSHX group (Supplementary Figs. 5A–5C). Under NDUFS4^{TG} circumstances, si-DUSP1 had a greater effect on cell activity and mitochondrial respiration than ad-DUSP1. Inhibiting mitophagy with 3MA reduced ATP generation and respiratory function in the ZSHX group (Supplementary Figs. 5D and 5E). In terms of the regulation of the expression level and gene transcription level of mitochondria related proteins (PINK/Parkin/ATG5), Ad-DUSP1/NDUFS4^{TG} did not affect the therapeutic effect of the drug, while si-DUSP1/NDUFS4^{TG} abolished the regulatory effect of the drug on mitophagy (Supplementary Figs. 5F and 5G).

3.8. Kaempferol regulates ER stress-induced mitochondrial UPRs (mtUPRs) via DUSP1-NDUFS4

Immunofluorescence detection of ER expression revealed that green fluorescence intensity was reduced and cell activity decreased in the H/R group, whereas fluorescence intensity was increased and cell activity was restored in the ZSHX and Mots-C/FCCP/UA groups (Supplementary Figs. 6A–6C), implying that ZSHX ameliorated the ER membrane structure damage caused by I/R. The ZSHX intervention reduced the level of PERK/CHOP/ATF6/HSP10/HSP60/mtDNAj transcription in the I/R group, while Mots-C/FCCP/UA had the similar inhibitory effect on the

above molecules. However, mtUPR and ER stress factor transcript levels were higher in the 3MA and NDUFS4^{CKO} groups, while the difference was not statistically significant when compared to the I/R group (Supplementary Figs. 6D–6I). This demonstrates that inhibiting mitochondrial unfolded protein response drastically reduced ZSHX's protective effect on cardiomyocytes. The activation of mitochondrial unfolded protein response is the primary mechanism by which ZSHX achieves its therapeutic effect. Furthermore, Mots-C and FCCP were engaged in the regulation of ER stress and mitochondrial UPR. However, it is noteworthy that the therapeutic effect of the drug was abolished after NDUFS4 cardiac specific knockout (NDUFS4^{CKO}). Knockdown or overexpression treatment of DUSP1 (si-DUSP1/ad-DUSP1) did not change the elimination effect of NDUFS4 on drug treatment effect (Supplementary Figs. 6A–6I). It can be inferred from the experimental results that ndusf4 can interact with DUSP1 and affect the regulation of kaempferol on mitochondrial endoplasmic reticulum homeostasis.

4. Discussion

In this investigation, we integrated single-cell sequencing,

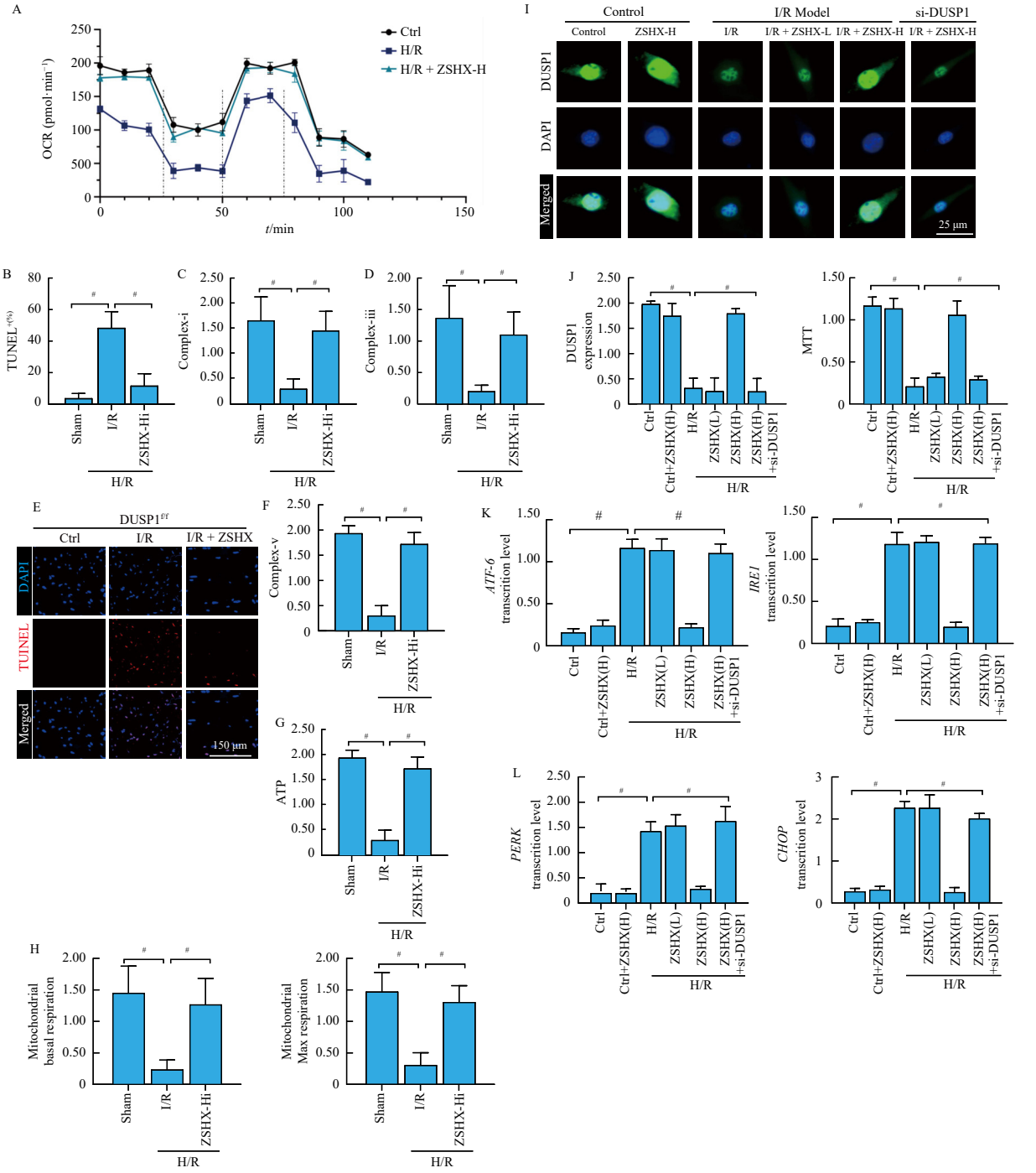

Fig. 7 (A) Cellular oxygen consumption rate (OCR) assay. (B, E) Apoptosis rate detected by TUNEL fluorescence staining. (C, D, F) Changes in mitochondrial respiratory chain complex activity in each group. (G) ATP production in the sham, I/R, and ZSHX-H groups. (H) Cellular respiratory function in the sham, I/R, and ZSHX-H groups. (I) Immunofluorescence staining for DUSP1 protein expression. (J) DUSP1 protein expression and MTT assay of cell viability in each group. (K, L) mRNA expression levels of *ATF6*, *IRE1*, *PERK*, and *CHOP*. Data are expressed as mean ± SD (n = 8 independent experiments). One-way ANOVA followed by Tukey's post hoc test was used to assess statistical significance. $^{\#}P < 0.05$ for the indicated comparisons.

network pharmacology, and *in vivo* and *in vitro* pharmacological interventions to elucidate the mechanisms by which ZSHX attenuates inflammatory injury in I/R myocardium. The study yielded three principal findings. First, ER stress induces mitochondrial metabolic reprogramming as an adaptive response during the inflammatory phase of MIRI. Second, activation of DUSP1 and NDUFS4 represents a critical mechanism through which ZSHX maintains mitochondrial protein homeostasis, promotes mitochondrial autophagy, and inhibits apoptosis. Third, kaempferol, a key bioactive component of ZSHX, allosterically modulates DUSP1 and NDUFS4 while concurrently suppressing ER stress and mitochondrial dysfunction.

This study employs a multidimensional analytical framework to comprehensively delineate how ZSHX regulates MIRI, a pathological process primarily driven by the interplay of immune cell activation, inflammation, mitochondrial dysfunction with metabolic dysregulation, ER stress, and autophagy. ZSHX exerts therapeutic effects by targeting central molecular nodes within this complex regulatory network. MIRI involves inflammatory crosstalk mediated by multiple mechanisms. Prior studies have demonstrated macrophage polarization and increased infiltration of monocytes and neutrophils in the immune response to I/R [24]. Inflammatory processes can trigger intracellular oxidative stress and activate ER stress and the UPR [25]. Activation of the ad-

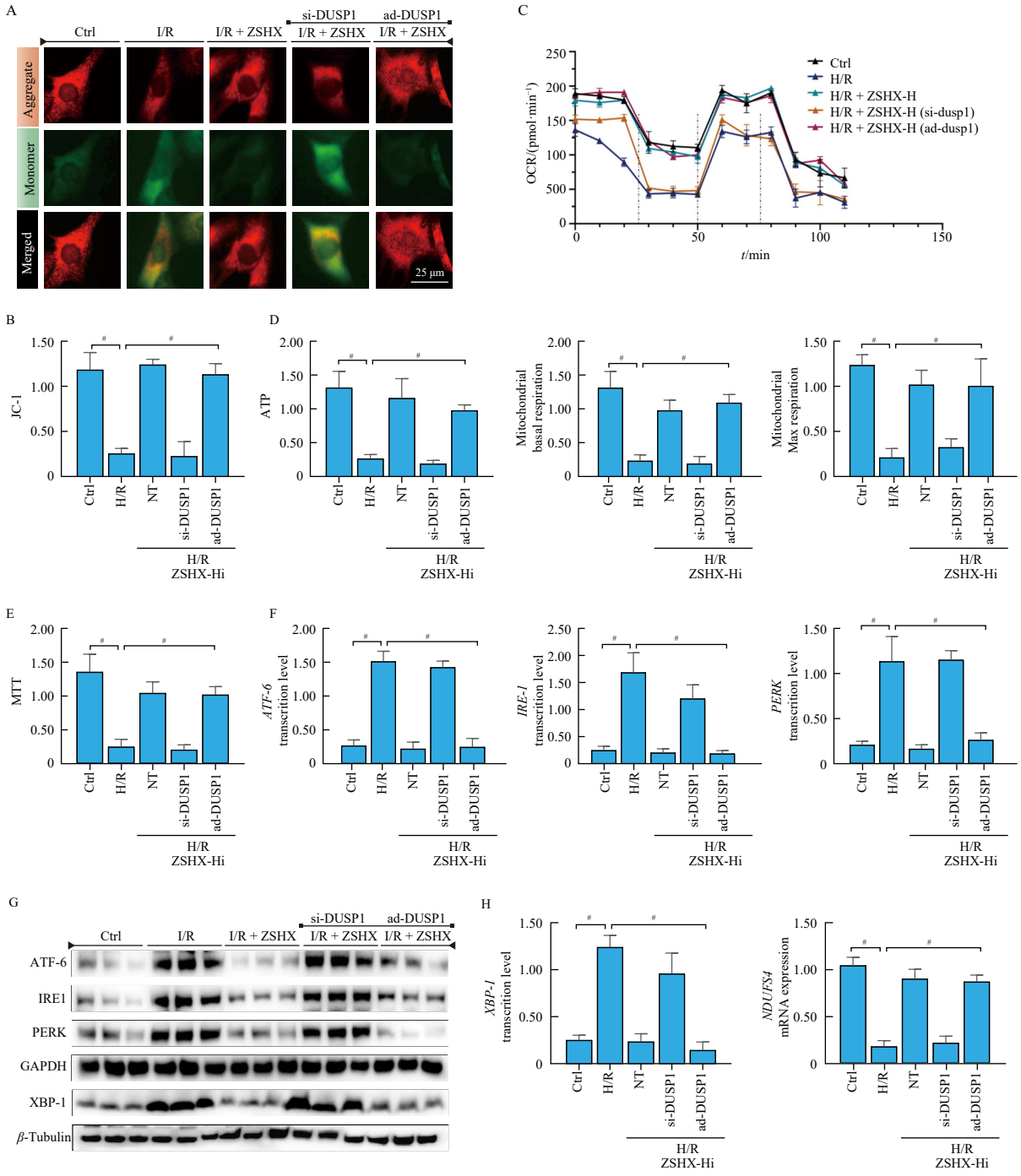

Fig. 8 (A) JC-1 staining for assessment of mitochondrial membrane potential. (B) Quantification of JC-1 aggregates reflecting mitochondrial membrane potential. (C) Cellular oxygen consumption rate (OCR) assay. (D) ATP content, basal mitochondrial respiration, and maximal mitochondrial respiration assays. (E) MTT assay of cell viability. (F) RT-PCR analysis of endoplasmic reticulum (ER) stress-related gene expression. (G) Western blot analysis of ER stress-related protein expression. (H) RT-PCR analysis of *XBP1* and *NDUFS4* mRNA levels. Data are expressed as mean ± SD (n = 8 independent experiments). One-way ANOVA followed by Tukey's post hoc test was used to assess statistical significance. $^{\#}P < 0.05$ for the indicated comparisons.

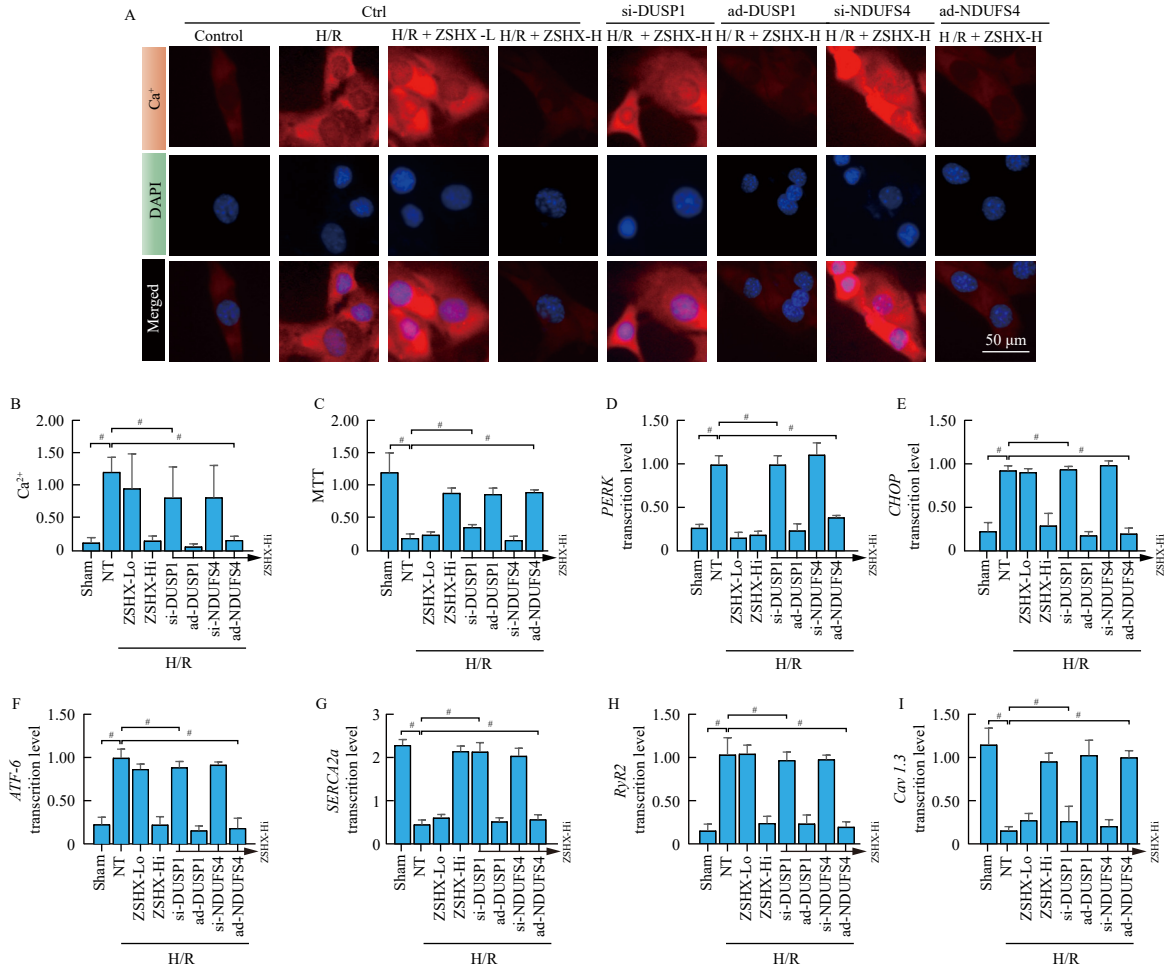

Fig. 9 (A) Ca^{2+} fluorescent probe specific staining analysis. (B) Ca^{2+} fluorescence quantitative assay. (C) MTT assay for cellular activity. (D, E) mRNA transcript levels of PERK/CHOP. (F) mRAN transcript levels of *ATF-6*. (G) mRNA transcript levels of *SERCA2a*. (H) mRNA transcript levels of *RyR2*. (I) mRNA transcript levels of *Cav 1.3*. Data are expressed as mean ± SD (n = 8 independent experiments). One-way ANOVA followed by Tukey's post hoc test was used to assess statistical significance. $^{\#}P < 0.05$ for the indicated comparisons.

aptive mtUPRs modulates the ER quality-control system and mitigates cellular stress damage [26]. Our previous work revealed that I/R induces myocardial inflammatory infiltrative injury by upregulating IL-6, IL-10, TNF-α, and Gr-1 expression and by activating mitochondrial oxidative stress [23, 27]. The present study further demonstrates that ER stress drives mitochondrial metabolic reprogramming as an adaptive mechanism in I/R-induced myocardial inflammation and identifies the DUSP1–NDUFS4 pathway as a key mediator.

In this study, single-cell sequencing was applied to examine the association between mitochondrial energy metabolism and cell death in the context of cardiac inflammation. Network pharmacology screening indicated that ZSHX modulates inflammation and cell death and regulates mitochondrial function. *In vitro* experiments showed that I/R injury induced significant accumulation of inflammatory factors, Gr-1, TNF-α, IL-17, and IL-18, alongside a consistent upregulation of ER stress-related proteins, including ATF6, PERK, and CHOP. This suggests that the inflammatory response is the primary pathological feature of I/R injury in cardiac tissue. ER stress and mitochondrial functional modulation represent coordinated, adaptive cellular responses to inflammation [28, 29]. Supplementary single-cell analyses revealed immunological interactions between inflammation and I/R injury, underscoring the pivotal role of macrophages in MI pathogenesis. Previous studies indicate that inflammatory glycolysis reprograms mitochondrial metabolic rhythms and impairs macrophage repair functions [30]. Our findings further show that deficiency in NDUFS4, a core subunit of mitochondrial respiratory Complex I, downregulates anti-inflammatory and tissue-repair factors, thereby promoting metabolic reprogramming and suppressing macrophage proliferation [19]. Additionally, I/R injury disrupts intracellular calcium homeostasis and impairs respiratory Complex I and III activity. Prior research has shown that ZSHX treatment significantly reduces mitochondrial oxidative stress and attenuates mitochondrial fission [31, 32]. ER stress perturbs calcium homeostasis, leading to ROS accumulation [33]. SERCA2a overexpression has been shown to inhibit hypoxia-induced ER stress [34]. In conjunction with these findings, the current study indicates that ZSHX upregulates SERCA2a, suppresses ER stress, reduces oxidative stress injury, and preserves mitochondrial function. Thus, modulation of ER stress is central to mitigating myocardial inflammatory damage.

Mitochondrial protein dysregulation disrupts metabolic reprogramming and impairs the activity of mitochondrial metabolic enzymes [35]. Following MI, macrophages shift their metabolic profile from inflammatory glycolysis to OXPHOS, a transition associated with reduced infarct size [36]. Inflammatory glycolysis has been shown to alter mitochondrial metabolic rhythms and counteract macrophage repair mechanisms. Metabolic substrate switching is a compensatory response to pathological cardiac remodeling. In recent years, mitochondrial metabolic reprogramming has emerged as a potential therapeutic strategy for heart failure and MI [35]. Single-cell sequencing in this study confirmed that DEGs were predominantly enriched in pathways related to material metabolism, mitochondrial respiration, and programmed cell death, particularly in macrophages and fibroblasts.

Metabolomic analyses revealed that ZSHX intervention altered the content and expression of metabolites in the I/R group. *In vitro* data indicated that ZSHX influences mitochondrial respiratory activity and modifies mitochondrial metabolic pathways. Therefore, we infer that the substantial release of Gr-1, TNF-α, and IL-17 following I/R injury triggers ER stress. Concurrently, cardiomyocyte metabolic characteristics are also altered. In response to I/R-induced inflammation, ZSHX modulates substance metabolic pathways and regulates cardiomyocyte metabolic reprogramming.

Overexpression of DUSP1 promotes maintenance of mitochondrial QC network homeostasis [37]. DUSP1 induces lethal mitochondrial fission in coordination with mitochondrial autophagy [15]. Moreover, DUSP1 attenuates the inflammatory response by reducing neutrophil infiltration and, in a dependent manner, inactivating JNK [38]. In I/R-injured myocardium, DUSP1 is known to preserve mitochondrial function. However, evidence linking DUSP1 to ER stress induction or direct regulation of mitochondri-

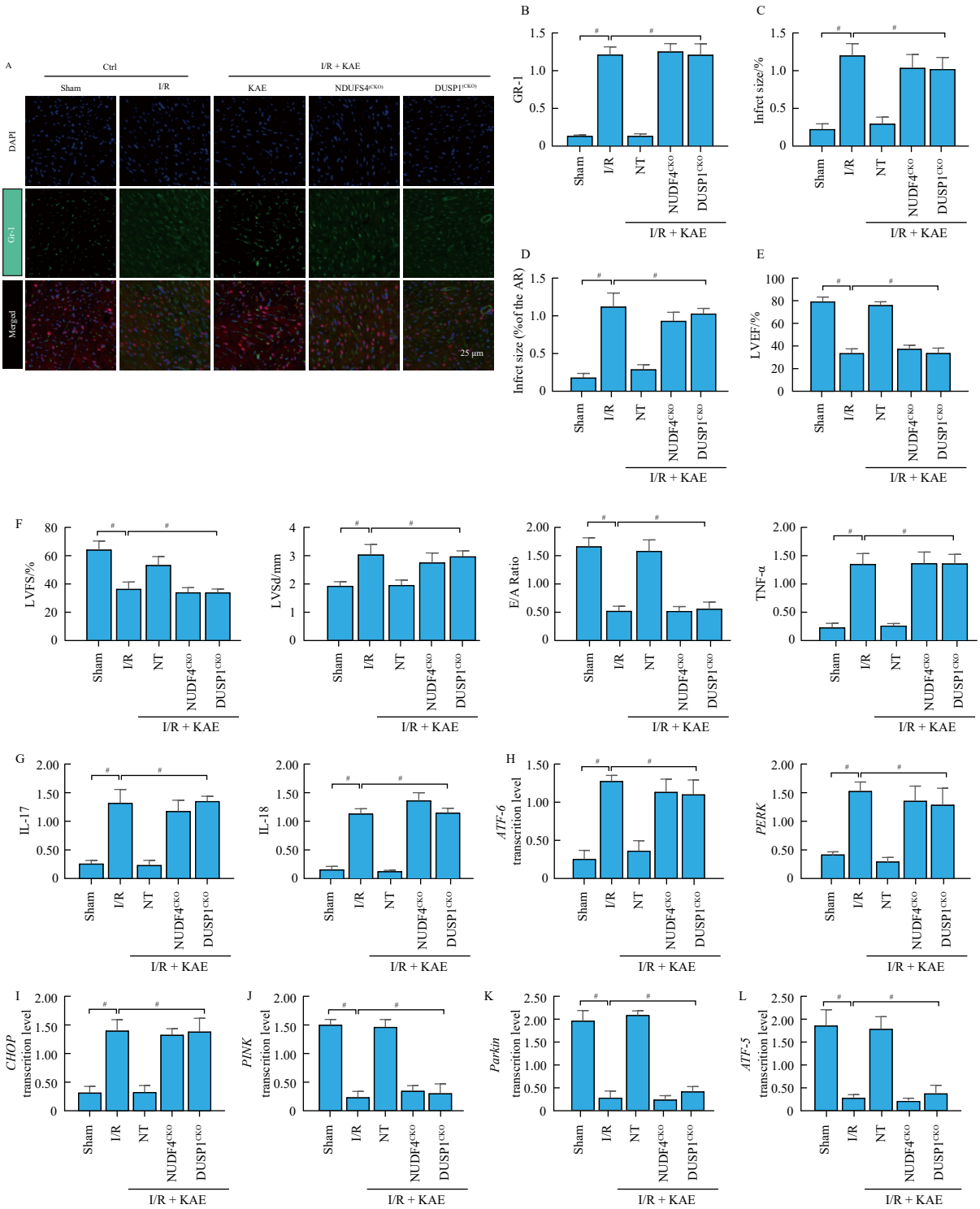

Fig. 10 (A, B) Quantitative immunofluorescence assay for Gr-1. (C, D) Percentage of myocardial infarction area. (E, F) Cardiac function parameters (LVEF%, LVFS%, LVsd, E/A ratio) and TNF-α levels. (G) Determination of IL-17 and IL-18 contents. (H) mRNA transcript levels of *ATF-6* and *PERK*. (I–L) mRNA transcript levels of *CHOP*, *PINK*, *Parkin*, and *ATG5*. Data are expressed as mean ± SD (n = 8 independent experiments). One-way ANOVA followed by Tukey's post hoc test was used to assess statistical significance. $^{\#}P < 0.05$ for the indicated comparisons.

al metabolic reprogramming remains limited. NDUFS4 is a structural component of mitochondrial respiratory Complex I. Deficiency in NDUFS4 downregulates anti-inflammatory and tissue repair factors, induces mitochondrial metabolic reprogramming, and inhibits macrophage phagocytosis [39]. Thus, NDUFS4 deficiency constitutes a maladaptive inflammatory response. In astrocytes, NDUFS4 loss enhances direct neural reprogramming and influences mitochondrial-ER stress crosstalk [40]. Could NDUFS4 similarly modulate the developmental trajectory of cardiomyocytes and rewire metabolic processes? This may facilitate cardiomyocyte regeneration following cardiac I/R injury. We therefore hypothesized that ZSHX regulates ER stress through coordinated action on DUSP1 and NDUFS4. Using adenoviral transfection, we established si-DUSP1, ad-DUSP1, si-NDUFS4, and ad-NDUFS4 cell models. The results support the coordinated regulation of mitochondrial metabolism and ER stress by DUSP1 and NDUFS4. Specifically, si-DUSP1 and si-NDUFS4 reversed ZSHX-mediated suppression of ER stress by reducing cellular activity and mitochondrial respiration. Furthermore, both DUSP1 and NDUFS4 regulate calcium homeostasis. As previously reported, ER stress disrupts ER calcium balance, resulting in ROS accumulation. In this study, we confirmed that ZSHX protects mitochondrial protein homeostasis and normal biological functions, inhibits ER stress injury, restores calcium cycling and release equilibrium, upregulates DUSP1 and NDUFS4 expression, and modulates mitochondrial metabolic reprogramming to alleviate myocardial inflammatory injury.

Finally, we used LC-MS to identify the active components of ZSHX and selected kaempferol for further investigation. Kaempferol is a bioactive constituent of Huoxin Pill, Tongguan capsule, and several other clinically used patented Chinese medicines for myocardial ischemia [41]. In addition to its high affinity for NLRP3, kaempferol protects against I/R-induced myocardial injury by modulating ER stress [42]. Molecular docking confirmed DUSP1 and NDUFS4 as kaempferol targets in mitigating MIRI. Using a gene-editing approach to generate $NDUFS4^{CKO}$/$DUSP1^{CKO}$ animal models, we found that kaempferol recapitulates the anti-inflammatory effects of ZSHX, including suppression of ER stress and activation of PINK/Parkin-mediated mitochondrial autophagy. These protective effects were abolished in $NDUFS4^{CKO}$/$DUSP1^{CKO}$ mice.

Upon examining the relationship between NDUFS4 and DUSP1, we observed that si-DUSP1 suppressed NDUFS4 expression. This suggests that NDUFS4 may act downstream of DUSP1 as an intermediary effector in mitochondrial regulation. Proteotoxic stress arises from disruptions in mitochondrial protein homeostasis [43], and a substantial influx of misfolded proteins into mitochondria triggers mitochondrial autophagy *via* pathways such as PINK/Parkin [44, 45]. We treated cells with 3MA, an autophagy inhibitor, and urolithin A, an autophagy agonist. The results demonstrated that kaempferol suppresses ER stress and the UPR by inducing mitochondrial autophagy. Conversely, si-DUSP1 abolished kaempferol's effect on mitochondrial autophagy. Motsc, a mitochondria-derived peptide with anti-inflammatory properties, was used in conjunction with FCCP to confirm that kaempferol suppresses inflammation and reprograms mitochondrial metabolism to initiate self-regulated protein homeostasis. ER stress activates the UPR signaling pathway, which can initiate various cell death mechanisms [19, 46]. Prolonged upregulation of ATF6 and CHOP further promotes the expression of pro-apoptotic proteins [47]. The present study shows that ZSHX alters cardiomyocyte material metabolism and prevents apoptosis resulting from mitochondrial dysfunction by activating mitochondrial autophagy, thereby preventing excessive ER stress and mtUPR activation.

This study indicates that I/R injury is associated with reduced or absent DUSP1 and NDUFS4 expression. Additionally, the surge in inflammatory mediators disrupts proteostasis, leading to ER stress and mitochondrial metabolic reprogramming. Kaempferol, the primary active component of ZSHX, suppresses inflammatory bursts, preserves mitochondrial function, activates protective mitochondrial autophagy, and upregulates DUSP1 and NDUFS4 expression following I/R injury. These findings support the synergistic regulation of protein homeostasis by the DUSP1–NDUFS4 axis, although further investigation is required to clarify their molecular interactions using immunoprecipitation and pull-down assays. *In vivo* validation studies are also warranted to confirm the *in vitro* observations. Timely supplementation of DUSP1 and NDUFS4 may reduce I/R-induced myocardial damage and promote cardiomyocyte regeneration by reprogramming mitochondrial metabolism, restoring protein homeostasis, and activating mitochondrial autophagy and respiration.

Several limitations should be acknowledged. First, although kaempferol was prioritized for mechanistic validation based on network pharmacology predictions and molecular docking, these analyses represent a systematic, stepwise approach to deconvoluting ZSHX's multi-component effects rather than an isolated focus. Nevertheless, the broader therapeutic synergy of ZSHX likely involves additive or compensatory interactions among other identified constituents (e.g., astragaloside A, tanshinone IIA), which should be rigorously evaluated in future combinatorial studies. Second, although this study emphasizes ER stress and mitochondrial metabolic reprogramming as central mechanisms, the inclusion of immunomodulation and autophagy reflects their pathophysiological interplay with these core pathways. Future multi-omics analyses should quantitatively resolve the temporal hierarchy and spatial interdependence of these processes.

5. Conclusion

Kaempferol, the primary active component of the ZSHX formula, attenuated MIRI by preserving mitochondrial function, suppressing the inflammatory response and ER stress, and upregulating DUSP1 and NDUFS4 expression.

Declarations

Ethics in publishing

This study was reviewed by the Ethics Center of Guang'anmen Hospital in accordance with the ARRIVE guidelines for animal experiments (approval number: IACUC-GAMH-2023-054-SQ).

Conflict of interests

These authors declare no conflict of interest.

Funding

This work was supported by the National Natural Science Foundation of China (No. 82305204), the Academic Inheritance and Communication Project of the China Academy of Chinese Medical Sciences (No. CI2022E012XB), the High Level Chinese Medical Hospital Promotion Project (No. HLCMHPP2023053), the Chinese Academy of Chinese Medical Sciences Doctoral Talents Training Fund (No. 2021), the Special Program for Training Outstanding Young Talents of the Chinese Academy of Traditional Chinese Medicine (No. ZZ16-YQ-021), and the Innovative Cultivation Project of Guang'anmen Hospital, Chinese Academy of Chinese Medical Sciences (No. 2022s481).

Supporting information

Supplementary data associated with this article can be requested by sending E-mail to the corresponding authors.

References

1 Anversa P, Sonnenblick EH. Ischemic cardiomyopathy: pathophysiologic mechanisms. *Prog Cardiovasc Dis*. 1990;33(1):49-70. https://doi.org/10.1016/0033-0620(90)90039-5.
2 Bansal SS, Ismahil MA, Goel M, et al. Dysfunctional and proinflammatory regulatory T-lymphocytes are essential for adverse cardiac remodeling in ischemic cardiomyopathy. *Circulation*. 2019;139(2):206-221. https://doi.org/10.1161/CIRCULATIONAHA.118.036065.
3 Moroni F, Gertz Z, Azzalini L. Relief of ischemia in ischemic cardiomyopathy. *Curr Cardiol Rep*. 2021;23(7):80. https://doi.org/10.1007/s11886-021-01520-4.
4 Chang X, Liu RX, Li RB, et al. Molecular mechanisms of mitochondrial quality control in ischemic cardiomyopathy. *Int J Biol Sci*. 2023;19(2):426-448. https://doi.org/10.7150/ijbs.76223.
5 Pang BX, Dong GT, Pang TL, et al. Emerging insights into the pathogenesis and therapeutic strategies for vascular endothelial injury-associated diseases: focus on mitochondrial dysfunction. *Angiogenesis*. 2024;27(4):623-639. https://doi.org/10.1007/s10456-024-09938-4.
6 Pang BX, Dong GT, Pang TL, et al. Advances in pathogenesis and treatment of vascular endothelial injury-related diseases mediated by mitochondrial abnormality. *Front Pharmacol*. 2024;15:1422686. https://doi.org/10.3389/fphar.2024.1422686.
7 Chang X, Liu JF, Wang YL, et al. Mitochondrial disorder and treatment of ischemic cardiomyopathy: potential and advantages of Chinese herbal medicine. *Biomed Pharmacother*. 2023;159:114171. https://doi.org/10.1016/j.biopha.2022.114171.
8 Oakes SA, Papa FR. The role of endoplasmic reticulum stress in human pathology. Annu Rev Pathol. 2015;10:173-194. https://doi.org/10.1146/annurev-pathol-012513-104649.
9 Ren J, Bi YG, Sowers JR, et al. Endoplasmic reticulum stress and unfolded protein response in cardiovascular diseases. *Nat Rev Cardiol*. 2021;18(7):499-521. https://doi.org/10.1038/s41569-021-00511-w.
10 Wiseman RL, Mesgarzadeh JS, Hendershot LM. Reshaping endoplasmic reticulum quality control through the unfolded protein response. *Mol Cell*. 2022;82(8):1477-1491. https://doi.org/10.1016/j.molcel.2022.03.025.
11 Mishra P, Chan DC. Metabolic regulation of mitochondrial dynamics. *J Cell Biol*. 2016;212(4):379-387. https://doi.org/10.1083/jcb.201511036.
12 de Beauchamp L, Himonas E, Helgason GV. Mitochondrial metabolism as a potential therapeutic target in myeloid leukaemia. *Leukemia*. 2022;36(1):1-12. https://doi.org/10.1038/s41375-021-01416-w.
13 Levoux J, Prola A, Lafuste P, et al. Platelets facilitate the wound-healing capability of mesenchymal stem cells by mitochondrial transfer and metabolic reprogramming. *Cell Metab*. 2021;33(2):283-299. e9. https://doi.org/10.1016/j.cmet.2020.12.006.
14 Pu XY, Zhang X, Liu JF, et al. Ginsenoside Rb1 ameliorates heart failure through DUSP-1-TMBIM-6-mediated mitochondrial quality control and gut flora interactions. *Phytomedicine*. 2024;132:155880. https://doi.org/10.1016/j.phymed.2024.155880.
15 Jin QH, Li RB, Hu N, et al. DUSP1 alleviates cardiac ischemia/reperfusion injury by suppressing the Mff-required mitochondrial fission and Bnip3-related mitophagy *via* the JNK pathways. *Redox Biol*. 2015;14:576-587. https://doi.org/10.1016/j.redox.2017.11.004.
16 Yue ZJ, Zhang YR, Zhang W, et al. Kaempferol alleviates myocardial ischemia injury by reducing oxidative stress *via* the HDAC3-mediated Nrf2 signaling pathway. *J Adv Res*. 2024;75:755-764. https://doi.org/10.1016/j.jare.2024.10.037.
17 Zou RJ, Shi WT, Chang X, et al. The DNA-dependent protein kinase catalytic subunit exacerbates endotoxemia-induced myocardial microvascular injury by disrupting the MOTS-c/JNK pathway and inducing profilin-mediated lamellipodia degradation. *Theranostics*. 2024;14(4):1561-1582. https://doi.org/10.7150/thno.92650.
18 Andersson KB, Finsen AV, Sjåland C, et al. Mice carrying a conditional Serca2 (flox) allele for the generation of Ca^{2+} handling-deficient mouse model. *Cell Calcium*. 2009;46(3):219-225. https://doi.org/10.1016/j.ceca.2009.07.004.
19 Chang X, Zhang Q, Huang Y, et al. Quercetin inhibits necroptosis in cardiomyocytes after ischemia-reperfusion *via* DNA-PKcs-SIRT5-orchestrated mitochondrial quality control. *Phytother Res*. 2024;38(5):2496-2517. https://doi.org/10.1002/ptr.8177.
20 Marfella R, D'Amico M, Di Filippo C, et al. Myocardial infarction in diabetic rats: role of hyperglycaemia on infarct size and early expression of hypoxia-inducible factor 1. *Diabetologia*. 2002;45(8):1172-1181. https://doi.org/10.1007/s00125-002-0882-x.
21 Hu K, Ertl G. Technical challenges in small animal models mimicking human ischemic cardiovascular diseases. *Cardiology Plus*. 2024;9(1):9-11. https://doi.org/10.1097/CP9.0000000000000072.
22 Cai C, Guo ZZ, Chang X, et al. Empagliflozin attenuates cardiac microvascular ischemia/reperfusion through activating the AMPKα1/ULK1/FUNDC1/mitophagy pathway. *Redox Biol*. 2022;52:102288. https://doi.org/10.1016/j.redox.2022.102288.
23 Chang X, Zhou SY, Liu JF, et al. Zishenhuoxue decoction-induced myocardial protection against ischemic injury through TMBIM6-VDAC1-mediated regulation of calcium homeostasis and mitochondrial quality surveillance. *Phytomedicine*. 2024;132:155331. https://doi.org/10.1016/j.phymed.2023.155331.
24 Fan Q, TaoR, Zhang H, et al. Dectin-1 contributes to myocardial ischemia/reperfusion injury by regulating macrophage polarization and neutrophil infiltration. *Circulation*. 2019;139(5):663-678. https://doi.org/10.1161/CIRCULATIONAHA.118.036044.
25 Li WY, Li W, Leng Y, et al. Ferroptosis is involved in diabetes myocardial ischemia/reperfusion injury through endoplasmic reticulum stress. *DNA Cell Biol*. 2020;39(2):210-225. https://doi.org/10.1089/dna.2019.5097.
26 Ajoolabady A, Kaplowitz N, Lebeaupin C, et al. Endoplasmic reticulum stress in liver diseases. *Hepatology*. 2023;77(2):619-639. https://doi.org/10.1002/hep.32562.
27 Chang X, Li YK, Liu JF, et al. *β*-Tubulin contributes to Tongyang Huoxue decoction-induced protection against hypoxia/reoxygenation-induced injury of sinoatrial node cells through SIRT1-mediated regulation of mitochondrial quality surveillance. *Phytomedicine*. 2023;108:154502. https://doi.org/10.1016/j.phymed.2022.154502.
28 Li YK, Yu JC, Li RB, et al. New insights into the role of mitochondrial metabolic dysregulation and immune infiltration in septic cardiomyopathy by integrated bioinformatics analysis and experimental validation. *Cell Mol Biol Lett*. 2024;29(1):21. https://doi.org/10.1186/s11658-024-00536-2.
29 Bettigole SE, Glimcher LH. Endoplasmic reticulum stress in immunity. *Annu Rev Immunol*. 2015;33:107-138. https://doi.org/10.1146/annurev-immunol-032414-112116.
30 Li CY, Liu CB, Zhang JF, et al. Pyruvate dehydrogenase kinase regulates macrophage polarization in metabolic and inflammatory diseases. *Front Immunol*. 2023;14:1296687. https://doi.org/10.3389/fimmu.2023.1296687.
31 Chang X, Zhou SY, Liu JF, et al. Zishen Tongyang Huoxue decoction (TYHX) alleviates sinoatrial node cell ischemia/reperfusion injury by directing mitochondrial quality control *via* the VDAC1-*β*-tubulin signaling axis. *J Ethnopharmacol*. 2024;320:117371. https://doi.org/10.1016/j.jep.2023.117371.
32 Liu RX, Chang X, Li J, et al. Zishen Huoxue Recipe potecting mitochondrial function of hypoxic/reoxygenated myocardial cells through mTORC1 signaling pathway. *Evid-Based Compl Alt*. 2020;2020:8327307. https://doi.org/10.1155/2020/8327307.
33 De Stefani D, Bononi A, Romagnoli A, et al. VDAC1 selectively transfers apoptotic Ca^{2+} signals to mitochondria. *Cell Death Differ*. 2012;19(2):267-273. https://doi.org/10.1038/cdd.2011.92.
34 Dong JJ, Lu XC, Liu XH, et al. Effects of sarcoplasmic reticulum calcium ATPase 2a overexpression on endoplasmic reticulum stress in cardiomyocytes. *Chin Med J*. 2009;89(6):415-418. https://doi.org/10.3760/cma.j.issn.0376-2491.2009.06.020.
35 Lowery BJ, Jacobsen BS. Attributional analysis of chronic illness outcomes. *Nurs Res*. 1985;34(2):82-88. https://doi.org/10.1097/00006199-198503000-00004.
36 Zhang S, Zhang YK, Duan XW, et al. Targeting NPM1 epigenetically promotes postinfarction cardiac repair by reprogramming reparative macrophage metabolism. *Circulation*. 2024;149(25):1982-2001. https://doi.org/10.1161/CIRCULATIONAHA.123.065506.
37 Zhu H, Wang J, Xin T, et al. DUSP1 interacts with and dephosphorylates VCP to improve mitochondrial quality control against endotoxemia-induced myocardial dysfunction. *Cell Mol Life Sci*. 2023;80(8):213. https://doi.org/10.1007/s00018-023-04863-z.
38 Hu YC, Zhan F, Wang Y, et al. The Ninj1/Dusp1 axis contributes to liver ischemia reperfusion injury by regulating macrophage activation and neutrophil infiltration. *Cell Mol Gastroenterol Hepatol*. 2023;15(5):1071-1084. https://doi.org/10.1016/j.jcmgh.2023.01.008.
39 Cai SS, Zhao MY, Zhou B, et al. Mitochondrial dysfunction in macrophages promotes inflammation and suppresses repair after myocardial infarction. *J Clin Invest*. 2023;133(4):e159498. https://doi.org/10.1172/JCI159498.
40 Sonsalla G, Malpartida AB, Riedemann T, et al. Direct neuronal reprogramming of NDUFS4 patient cells identifies the unfolded protein response as a novel general reprogramming hurdle. *Neuron*. 2024;112(7):1117-1132. e9. https://doi.org/10.1016/j.neuron.2023.12.020.
41 Cao C, Qi YT, Wang AA, et al. Huoxin Pill reduces myocardial ischemia reperfusion injury in rats *via* TLR4/NF-κB/NLRP3 signaling pathway. *Chin J Integr Med*. 2023;29(12):1066-1076. https://doi.org/10.1007/s11655-023-3640-1.
42 Kim DS, Ha KC, Kwon DY, et al. Kaempferol protects ischemia/reperfusion-induced cardiac damage through the regulation of endoplasmic reticulum stress. *Immunopharmacol Immunotoxicol*. 2008;30(2):257-270. https://doi.org/10.1080/08923970701812530.
43 Zhang XH, Shi SQ, Du YH, et al. Shaping cardiac destiny: the role of post-translational modifications on endoplasmic reticulum-mitochondria crosstalk in cardiac remodeling. *Front Pharmacol*. 2024;15:1423356. https://doi.org/10.3389/fphar.2024.1423356.
44 Zhang X, Zhou H, Chang X. Involvement of mitochondrial dynamics and mitophagy in diabetic endothelial dysfunction and cardiac microvascular injury. *Arch Toxicol*. 2023;97(12):3023-3035. https://doi.org/10.1007/s00204-023-03599-w.
45 Wang JY, Zhuang HW, Jia LQ, et al. Nuclear receptor subfamily 4 group A member 1 promotes myocardial ischemia/reperfusion injury through inducing mitochondrial fission factor-mediated mitochondrial fragmentation and inhibiting FUN14 domain containing 1-depedent mitophagy. *Int J Biol Sci*. 2024;20(11):4458-4475. https://doi.org/10.7150/ijbs.95853.
46 An YJ, Wang XS, Guan XJ, et al. Endoplasmic reticulum stress-mediated cell death in cardiovascular disease. *Cell Stress Chaperones*. 2024;29(1):158-174. https://doi.org/10.1016/j.cstres.2023.12.003.
47 Lee JH, Kwon EJ, Kim DH. Calumenin has a role in the alleviation of ER stress in neonatal rat cardiomyocytes. *Biochem Biophys Res Commun*. 2013;439(3):327-332. https://doi.org/10.1016/j.bbrc.2013.08.087.